CARDIFF UNIVERSITY
PRIFYSGOL CAERDYDD

ORCA – Online Research @ Cardiff

This is an Open Access document downloaded from ORCA, Cardiff University's institutional repository:https://orca.cardiff.ac.uk/id/eprint/159135/

This is the author's version of a work that was submitted to / accepted for publication.

Citation for final published version:

Shao, Longyi, Hua, Fanghui, Wang, Juan, Ji, Xingkai, Yan, Zhiming, Zhang, Tianchang, Wang, Xuetian, Ma, Shimin, Jones, Tim and Lu, Huinan 2023. Palynological dynamics in the late Permian and the Permian-Triassic transition in southwestern China. Palaeogeography, Palaeoclimatology, Palaeoecology 619 , 111540. 10.1016/j.palaeo.2023.111540

Publishers page: http://dx.doi.org/10.1016/j.palaeo.2023.111540

Please note:
Changes made as a result of publishing processes such as copy-editing, formatting and page numbers may not be reflected in this version. For the definitive version of this publication, please refer to the published source. You are advised to consult the publisher's version if you wish to cite this paper.

This version is being made available in accordance with publisher policies. See http://orca.cf.ac.uk/policies.html for usage policies. Copyright and moral rights for publications made available in ORCA are retained by the copyright holders.

Palynological dynamics in the Late Permian and the Permian–Triassic transition in southwestern China

Longyi Shao[1*], Fanghui Hua[1], Juan Wang[1,3], Xingkai Ji[2*], Zhiming Yan[1,4], Tianchang Zhang[1], Xuetian Wang[1], Shimin Ma[1], Tim Jones[5], Huinan Lu[2]

1 College of Geoscience and Surveying Engineering, China University of Mining and Technology (Beijing), Beijing 100083, China
2 Nanjing Institute of Geology and Palaeontology, Chinese Academy of Sciences, Nanjing 210008, China
3 School of Resources and Environment, Henan Polytechnic University, Jiaozuo 454003, Henan Province, China
4 Institute of Architectural Engineering, Weifang University, Weifang 261061, Shandong Province, China
5 School of Earth and Environmental Sciences, Cardiff University, Cardiff, CF10, 3YE, Wales, UK
* Email: ShaoL@cumtb.edu.cn; xkji@nigpas.ac.cn

Highlights:

- Four palynological assemblages spanned the Late Permian and the Permian–Triassic transition in SW China
- The *gigantopterid* peat-forming forests diminished abruptly at the end-Permian
- The terrestrial floral extinction is a two-staged and long-duration event in SW China
- Upland gymnosperm forests increase in the earliest Triassic

Abstract: The Permian-Triassic mass extinction (PTME) is regarded as the largest biotic crisis of the Phanerozoic. However, the influence of the terrestrial ecological disturbance on plants remains controversial. Here we study the Late Permian to the Early Triassic palynological successions from three borehole sections drilled through the entire Lopingian (the Late Permian) and the Permian–Triassic transitional strata in southwestern China. Analyses of palynomorph composition and relative abundance allow us to identify four distinct palynofloral assemblages, which include, in ascending order, *Tripartites cristatus* var. *minor* - *Torispora laevigata* (ML) assemblage, the *Crassispora orientalis* - *Anticapipollis tornatilis* (OT) assemblage, *Lundbladispora communis* - *Aratrisporites yunnanensis* (CY) assemblage, and *Pteruchipollenites reticorpus* - *Protopinus fuyuanensis* (RF) assemblage. These palynological assemblages, together with recently updated age data, further improve our understanding of vegetation dynamics around the PTME. The ML and OT assemblages from the Xuanwei Formation are dominated by ferny rainforest and reflect warm and humid paleoclimate conditions preceding the PTME. At the bottom of the overlying Kayitou Formation, the abrupt replacement of the diverse sporomorph assemblage by the assemblage containing herbaceous communities reveals a dramatic floral disruption. The CY assemblage from the bottom part of the Kayitou Formation marks the destruction of *Gigantopteris* peat-forming ecosystems, and only a few species of *Gigantopteris* were retained in this assemblage. Subsequently, in the Kayitou Formation notable quantities of gymnosperm pollen dominate the RF assemblage. Many gymnosperms from the RF assemblage were present in the older assemblages in low abundances but they persisted through the ecological disturbance interval and rebounded in the early Triassic RF assemblage. The drought-tolerant plants growing in uplands were likely the first batch of plants to adapt and recover after the extinction event. In the upper part of the Kayitou Formation and the lower part of the Dongchuan Formation, spore and pollen fossils are absent, which may suggest the collapse of the local terrestrial ecosystem and may also indicate unsuitable conditions for microfossil preservation. We conclude that the PTME caused a sharp decrease in plant species and changes in vegetation-community compositions, but it did not immediately eradicate the terrestrial ecosystem in southwestern China. This observation supports the hypothesis that the extinction process of terrestrial vegetation was a two-staged and longer-duration event in southwestern China.

Keywords: Terrestrial Permian–Triassic boundary; palynological profiles; mass extinction; southwestern China;

1. Introduction

The Permian-Triassic transition is an important period in the Earth's evolutionary history (Benton and Newell, 2014). S

The statistical analyses of abundant fossil evidence supports the view that marine faunas suffered from a rapid and catastrophic extinction (Shen S Z et al., 2011; Burgess et al., 2014; Li et al., 2016; Shen S Z et al., 2019). In contrast, the corresponding record of plant fossils during this interval is sporadic and relatively incomplete, and the extinction patterns recognised among fossil plants at the PTME have not been unified (Dal Corso et al., 2022). Some authors argued that the terrestrial plants had a loss of diversity with a magnitude that is comparable to the losses seen in the marine extinction (Rees., 2002; Benton and Newell, 2014). The study of the global-scale evolution of fossil plant families indicates that the low-latitude *Gigantopteris* floras (Yu et al., 2015; Xu et al., 2022) and the southern high-latitude *Glossopteris* flora (Fielding et al., 2019) disappeared around the time of the Permian-Triassic boundary. Some studies even propose an earlier onset of the terrestrial crisis relative to the marine extinction (Fielding et al., 2019; Wignall et al., 2020; Chu et al., 2020). There are other studies suggesting that the extinction of plants was a gradual process (Xiong and Wang, 2016), with the process being a gradual extinction of plants followed by a final catastrophic stage (Xu et al., 2022). A study by Nowak et al. (2019) even advocates that there was no mass extinction for land plants across the Permian–Triassic transition, and that the diversities of gymnosperm macrofossils and also the pollen had even increased.

The palynomorph fossil record can provide continuous evidence of floras and promotes a unified understanding of global life events (Peng et al., 2006; Yuan et al., 2014; Liu et al., 2020; Spina et al., 2015). High-resolution palynological research in many continuous non-marine sections has been conducted (Fielding et al., 2019; Ouyang, 1982; Peng et al., 2006; Broutin et al., 2020; Liu et al, 2020). It was found that various regions showed varying degrees of decline in plant diversity in the Permian-Triassic transition (Schneebeli-Hermann and Bucher, 2015; Xiong et al., 2021; Liu et al, 2020; Xu et al., 2022). This may be due to the fact that the environmental changes caused by the PTME varied from region to region (Liu et al., 2020; Xu et al., 2022). Some of these studies have revealed a rapid recovery of various species in some regions following the decline in plant diversity (Liu et al, 2020; Hochuli et al., 2010; Vajda et al., 2020). It is apparent that these different scenarios are induced by inconsistent stratigraphic dating in different regions, hence the palynological investigations in a more precise time frame are essential in distinguishing whether the plant episodic evolutions occurred before, during or after extinction events.

Southwestern China possessed a stable peatland ecosystem in the Late Permian, which was the ultimate refuge of the Paleozoic fern flora (Broutin et al., 2020). The tropical rainforests dominated by *Gigantopteris* in the low paleolatitudes were the main contributor to the Late Permian coals in southwestern China (Peng et al., 2006; Yu et al., 2015). Plant macrofossil studies have found that the regionally expansive and diverse *Gigantopteris* flora was replaced by a limited diversity of lycopsid flora in the bottom part of the Kayitou Formation (Bercovici et al., 2015; Yu et al., 2015; Zhang et al., 2016; Xu et al., 2022). Plant diversity substantially declined resulting in reduced sequestration of organic matter and the subsequent coal gap (Shao et al., 2020; Retallack et al., 1996). However, the palynology of the Late Permian–Early Triassic succession in southwestern China indicated that moderately rich Palaeozoic palynomorphs persisted after the uppermost coal of the Xuanwei Formation and extended through the earliest Triassic, which presents evidence for no floral mass extinction at the PTME (Ouyang, 1982; Xiong and Wang, 2016; Nowak et al., 2019). In addition, the position of the Permian-Triassic boundary (PTB) and the extinction interval in terrestrial sections are still controversial in southwestern China (Zhang et al., 2016; Chu et al., 2020). High-resolution chemostratigraphy and high-precision age dating in southwestern China suggested that the position of the PTB in terrestrial sections is variable in different localities (Fig 1), occurring in the lower part of the Kayitou Formation (Chu et al., 2016; Zhang et al., 2016; Wignall et al., 2020) or near the top of the Kayitou Formation (Zhang et al., 2021). It is apparent that challenges in the identification of the PTB and the correlations in terrestrial sections have led to significant debate on the timing and nature of the PTME (Xiong and Wang, 2016; Wignall et al., 2020; Xu et al., 2022). Hence, a better understanding of the changes in terrestrial ecosystems requires more detailed and complete biostratigraphic study, especially those conducted at a regional scale.

In this investigation, a detailed palynological study was undertaken on 50 core samples collected in Fuyuan, eastern Yunnan Province, and a palynostratigraphic analysis of microfloral assemblages across the entire Lopingian (Late Permian) and the Permian-Triassic boundary is presented. Based on these palynological data, the factors resulting in the demise of certain terrestrial plants are further scrutinized. These results could provide new insights into the floristic changes associated with terrestrial environment perturbations across the Permian-Triassic boundary.

2. Geological setting

The study area is located in eastern Yunnan Province, which was a part of the western margin of the South China Plate during the Late Permian and the Early Triassic (Fig. 2). Siliciclastic sediments in this area were supplied predominantly from the Kangdian Oldland to the west, a large area of ancient crystalline rocks reduced to low relief by lengthy erosion through the Late Paleozoic, which was significantly affected by Emeishan mantle plume activity (He Bin et al., 2006; Wang X T et al., 2020). The paleo-latitudes of the South China Plate were equatorial, migrating northward from 4.5°S at 291.1 Ma (million years ago) during the Early Permian to 0.3°S at 251.9 Ma at the Permian-Triassic boundary (Domeier and Torsvik, 2014).

The Late Permian to the Early Triassic strata in southwestern China are subdivided into the Xuanwei, Kayitou, and Dongchuan Formations in ascending order (Shao et al., 2013; Shen et al., 2011; Zhang et al., 2016) (Fig. 1). Controlled by transgressions from the east throughout the Late Permian and the Early Triassic, the sedimentary environments in eastern Yunnan and western Guizhou vary from marine, transitional to terrestrial facies from east to west. The Xuanwei Formation and Kayitou Formation are dominated by terrestrial fluvial facies (Shao et al., 1998; Wang et al., 2011; Bercovici et al., 2015).

The Xuanwei Formation rests unconformably on the Emeishan Basalt Formation and is the last coal-bearing strata before the PTME. It mainly consists of gray to dark gray mudstone, siltstone, sandstone and includes multiple layers of coal (Shao et al., 1998, 2013; Wang et al., 2011). The sediments of the Xuanwei Formation were deposited in continental fluvial plain environments with locally developed transitional delta plain environments (Shao et al., 1998, 2013; Wang et al., 2020b). Paleoclimates were generally humid, supporting the development of diverse tropical rainforests of the *Gigantopteris* flora (Bercovici et al., 2015; Yu et al., 2015; Feng et al., 2018; Xu et al. 2022). With the top of the uppermost coal layer as the boundary, the Xuanwei Formation is conformably overlain by the Kayitou Formation (Shao et al., 2015).

The Kayitou Formation is composed of grayish-green fine-grained siliciclastic rocks (Bercovici et al., 2015; Zhang et al., 2016). Coals are absent in the Kayitou Formation and there are few macroplant fossils other than sporadic occurrences of *Gigantopteris*, *Peltaspermum* and *Tomiostrobus* (≈ *Annalepis*) at the base (Yu et al., 2015; Feng et al., 2020; Xu et al., 2022), and abundant *Euestheria* and *Palaeolimnadia* faunal communities (Chu et al., 2016). Chemical stratigraphic studies on continental and transitional facies sections in south China have shown that sharp negative excursions of carbon isotopes occurred in the Kayitou Formation, which was accompanied by an increase in Hg content of volcanic origin (Cui et al., 2017; Shen J et al., 2019; Zhang et al., 2016; Chu et al., 2019) (Fig.1).

The overlying Dongchuan Formation has a conformable contact with the Kayitou Formation, and its lithologies consist of red, fine-grained siliciclastic rocks. This formation was formed in non-marine braided fluvial environments under an arid paleoclimate, which favored a lack of organic matter, and almost no fossils (Bercovici et al., 2015; Shen et al., 2011; Zhang et al., 2016).

3. Materials and methods

Sampling for the palynological study was undertaken from mudstone (clay-sized component is more than 50%) and siltstone (silt-sized component is more than 50%) layers. A total of 54 rock samples were collected from cores of the 7806, 5101, and SC-1 boreholes in Fuyuan, eastern Yunnan Province. In the laboratory, the samples were crushed, weighed (100g for each sample), and treated with hydrochloric (HCl) and then hydrofluoric (HF) acids to remove carbonates and then silicates (Wood et al., 1996). The undissolved material consisted of sporopollen and other organic residues. These residues were centrifuged and sieved with a 5μm nylon mesh. Four sample-loaded glass slides (20×20mm) were made for each sample, and the fossils were identified under a biological binocular microscope with transmitted light. For each spore-pollen sample, more than 100 sporomorphs were identified by the point-counting method. Percentages of spore and pollen taxa were calculated based on the sum of total sporomorphs. The analysis of the samples was undertaken at the Nanjing Institute of Geology and Palaeontology of the Chinese Academy of Sciences. The recorded fossil types and percentages are shown in Table S1. Palynological assemblages were recognized by stratigraphically constrained cluster analysis (CONISS) on relative abundances of various palynomorph taxa in each sample using the *Tilia* software.

4. Results

Abundant well-preserved palynology fossils were found in 47 of the samples, while either no or only sporadic fossils were found in the other 7 samples. A total of 119 species in 80 genera were identified, along with some unrecognized taxa. According to the vertical distribution of the palynological species and CONISS cluster analysis on the relative abundance of various palynomorph taxa in each sample four palynomorph assemblages are defined by a straight cut of the dendrogram of total dispersion (Fig 3). In ascending stratigraphic order, these are referred to as the *Tripartites cristatus* var. *minor-Torispora laevigata* (ML) assemblage, the *Crassispora orientalis-Anticapipollis tornatilis* (OT) assemblage, the *Lundbladispora communis-Aratrisporites yunnanensis* (CY) assemblage, and the *Pteruchipollenites reticorpus-Protopinus fuyuanensis* (RF) assemblage. The dendrogram of mean within-cluster dispersion shows the relative homogeneity of the zones (Fig. 3).

4.1. ML assemblage

The ML assemblage is the first palynomorph assemblage in the lower part of the Xuanwei Formation, immediately above the Emeishan Basalt Formation. In this assemblage, pteridophyte spores are dominant, with the number percentage ranging from 96.08% to 98.76%, averaging 97.87%. The other component in this assemblage is gymnosperms pollen, which is scarce, ranging from 1.24% to 3.92%, with an average of 2.13%.

Among the spores in the ML assemblage, the cingulate trilete spores are the most abundant (31.53–54.04%, averaging 39.77%), followed by the non-cingulate trilete spore (32.09–45.01%, averaging 37.12%), with the monolete spores being the least common. The cingulate trilete spores include auriculate spores (*Triquitrites sinensis*, *T. rugulatus*, *Tripartites cristatus* var. *minor*), cingulate spores (*Densosporites anulatus*, *Propterisispora verruculifera*, *P. sparsus*), membranate spores (*Wilsonisporites radiatus*), patina spores (*Crassispora orientalis*). The non-cingulate trilete spores include spores with sculpture (14.91–32.02%, averaging 22.0%) and *leiotriletes* (10.82–21.43%, averaging 15.13%). The monolete spores include *Torispora laevigata*, *T. securis*, *T. verrucosa, Thymospora mesozoica*, *Punctatosporites scabellus, Laevigatosporites minimus and Yunnanospora radiate* (Fig. 4).

Gymnosperm pollen is not common and is only sporadically found in this assemblage, including *Florinites florini*, *Vesicaspora*, *Pityosporites*, *Anticapipollis tornatilis*, *Urmites* and *Cycadopites.*

4.2. OT assemblage

The OT assemblage occurs in the upper part of the Xuanwei Formation, and in this assemblage, pteridophyte spores are still dominant, ranging from 62.45% to 97.63%, with an average of 86.20%. The gymnosperm pollen is still less common, ranging from 2.37% to 37.55%, with an average of 13.80%.

Among the spores, the non-cingulate trilete spores are the most abundant (25.82 – 75.68%, averaging 45.16%), followed by the cingulate trilete spores (10.29 – 43.79%, averaging 26.80%), with the monolete spores being the least abundant (4.23–22.74%, averaging 14.24%). The non-cingulate trilete spores consist mainly of *Granulatisporites adnatoides*, *G. brachytus*, *Cyclogranisporites pressus*, *C. micaceus*, *C. microgranus*, *Converrucosisporites, Leiotriletes Concavus, L. exiguous, L.*

cyathidites, Waltzispora strictura, and *Dictyophyllidites mortoni*. The cingulate trilete spores are mainly the zonate spores (*Propterisispora verruculifera*, *P. sparsus*) and patinate spores (*Crassispora minuta*, *C. orientalis*), followed by the auriculate spores (*Tripartites cristatus* var. *minor, Triquitrites attenuates*, *T. rugulatus*). The monolete spores include *Laevigatosporites minimus*, *Torispora laevigata*, *Punctatosporites scabellus* and *Thymospora.*

Although the gymnosperm pollen was less common in the OT assemblage, its abundance and diversity are higher than those found in the ML assemblage. The non-taeniate bisaccates of the gymnosperm pollen are common, in which *Anticapipollis tornatili* is the most abundant species, followed by a moderate content of *Alisporites*, *Platysaccus*, *Piceaepollenites*, *Vitreisporites parvus*, *Klausipollenites* and *Pityosporites*, with the monosaccates, taeniate bisaccates, and monocolpates having the lowest abundances, being 1.42 %, 0.98% and 2.54%, respectively (Fig. 5).

The OT assemblage is a continuation of the ML assemblage and the difference between the two assemblages is mainly in the increased diversity of gymnosperm pollen in the OT assemblage. The ML assemblage contains six gymnosperm pollen genera, while the OT assemblage has 18 genera. It is noteworthy that the *Anticapipollis* content in the OT assemblage is significantly increased to between 0.5% and 9.34%. Furthermore, typical Early Triassic taxa are present in the OT assemblage, including *Lundbladispora*, *Aratrisporites, Dictyophyllidites* and *Neoraistrickia.*

4.3. CY assemblage

The CY assemblage occurs in the bottom part of the Kayitou Formation. In this assemblage, pteridophyte spores are still dominant, with the number percentage ranging from 92.09 to 98.20%, averaging 95.61%. The gymnosperms pollen range from 1.80% to 7.91%, averaging 4.39%.

The identified spore fossils include cingulate trilete, monoletes and non-cingulate trilete spores. The cingulate trilete spores are the most abundant (39.87% – 47.76%, averaging 44.49%), with the main species including *Lundbladispora communis*, *L. subornata* and *L. minima*. These species not only have larger number concentrations but also have a vertically continuous distribution. *Tripartites cristatus* var. *minor*, *Lycospora*, *Densosporites anulatus*, *Propterisispora verruculifera* and *Kraeuselisporites* have lower concentrations and a vertically discontinuous distribution. The Monoletes component ranges from 21.56 to 40.64%, averaging 33.61%, with the species less diverse and comprising almost exclusively of *Aratrisporites minimus* and *A. yunnanensis*. Non-cingulate trilete spores range from 9.16–30.54%, averaging 17.51%, with the common taxa including *Leiotriletes cyathidites*, *Concavisporites*, *Punctatisporites minutus* and *Cyclogranisporites micaceus*.

Gymnosperm pollen is also scarce, being represented by monosaccate, taeniate bisaccate pollen, non-taeniate bisaccate, and monocolpates. The main genera are *Vesicaspora*, *Protohaploxypinus*, *Gardenasporites*, *Alisporites*, *Protopinus fuyuanensis*, *Pityosporites* and *Cycadopites* (Fig. 6).

The fossil abundance and diversity in the CY assemblage have significantly decreased compared to the ML and OT assemblages. This observation suggests that the lower diversity is related to floral mass extinction. However, the lycopod spores of the gymnosperms, including *Lundbladispora* and *Aratrisporites*, are relatively abundant, which is consistent with the study of plant macrofossils for a post-extinction initial lycopod-dominated communities (Bercovici et al., 2015; Feng et al., 2020; Xu et al., 2022).

4.4. RF assemblage

The RF assemblage occurs in the lower part of the Kayitou Formation and in this assemblage, the gymnosperm pollen become the dominant group replacing pteridophyte spores. The gymnosperm pollen accounts for 53.85 to 85.88%, averaging 68.19%, and the pteridophyte spores and pteridosperm pollen account for 14.12 to 46.15%, averaging 31.81%.

The identified spores are predominantly non-cingulate trilete spores, with less abundant cingulate trilete and monolete spores. The non-cingulate trilete spores are the most abundant with the number percentage ranging from 10.0 to 41.03%, averaging 27.12%. The common species include *Leiotriletes cyathidites*, *Waltzispora* *strictura*, *Punctatisporites*, *Dictyophyllidites mortoni*, *Calamospora pallida*, *Granulatisporites*, and *Cyclogranisporites micaceus*. The cingulate trilete and monolete spores are less abundant, with the number percentage ranging from 0.59 to 3.42% (average 1.45%), and from 0.17 to 6.51% (average 3.24%), respectively. The common species include *Densosporites anulatus*, *Crassispora orientalis, Laevigatosporites*, *Torispora laevigata*, *Punctatosporites minutus*, and *Aratrisporites* sp.

The gymnosperm pollen microfossils are dominated by non-taeniate bisaccates, with a few monosaccites and monocolpates. The non-taeniate bisaccates have a higher number percentage of 48.72–68.82%, averaging 60.70%, including *Alisporites auritus*, *Protopinus fuyuanensis*, *P. asymmetricus*, *Platysaccus papilionis*, *Pteruchipollenites reticorpus*, *Abietineaepollenites sp.*, *Klausipollenites sp.*, and *Pityosporites sp.* The monosaccites and monocolpates occur sporadically, including species of *Protohaploxypinus*, *Gardenasporites*, *Lunatisporites, Vesicaspora* and *Urmites* (Fig. 7).

Compared with the CY assemblage, the species abundance in the RF assemblage obviously increases, reflected by an increase in gymnosperms pollen. These characteristics not only indicate that the extinction of terrestrial plants was not a sudden single process but also reflect the change in regional paleoclimates.

No palynological fossils are found in the upper part of the Kayitou Formation and the Dongchuan Formation.

5. Discussion

5.1. Palynological correlation

The ML assemblage dominated by pteridophyte spores and pteridosperm pollen possesses many elements of the Late Paleozoic *Gigantopteris* flora. The generic diversity of gymnosperm fossils is noticeably low (Broutin et al., 2020). This assemblage corresponds to the *Acrotorispora gigantea-Patellisporites meishanensis* (AP) assemblage proposed by Ouyang (1982), and the stratigraphical age approximately corresponds to the Wuchiapingian Stage (Fig 8). The overall composition of the ML assemblage is similar to the AP assemblage, both of which are characterized by abundant Cathaysian elements (Ouyang, 1982). However, in northern China, most of these Cathaysian elements gradually disappeared and were progressively replaced by Subangaran and Euramerican elements in the Late Permian (Broutin et al., 2020). The reason for this phenomenon can be attributed to the earlier occurrence of arid paleoclimate conditions in northern China (Zhu et al., 2020).

In the OL assemblage, more than 2/3rds of the species are also found in the ML assemblage, showing the Cathaysian flora still occupied a significant position. This assemblage corresponds to the *Lueckisporites virkkiae-Jugasporites schaubergeroides* assemblage proposed by Ouyang (1982), and the stratigraphic age approximately corresponds to the Changhsingian Stage. The amount of gymnosperm pollen in this interval increases, and typical Mesozoic floral elements start to appear. This palaeoflora became dominated by 'xerophytic' plants in northern China, where only a few Cathaysian relict plants were preserved (Broutin et al., 2020). The Mesozoic pioneer plants were identified in both southern and northern China landmasses. In southern Tibet, gymnosperm pollen dominated in the early Changhsingian *Scheuringipollenites ovatus–Vitreisporites pallidus* assemblage, similar to that found in the Liujiagou Formation in northern China (Liu et al., 2020). In southern Tibet, abundant *Reduviasporonites* fossils were observed in the late Changhsingian *Reduviasporonites catenulatus* assemblage, and this corresponded to a worldwide fungal peak (Rampino and Eshet, 2018). The fungal layer was also observed at the top of the Xuanwei Formation in terrestrial sections in southwestern China (Bercovici et al., 2015). In addition, the understory components of the *Dulhuntyispora Parvithola* zone in eastern Australia were dominated by the azonate trilete and zonate trilete spores, thus supporting this correlation (Fielding et al., 2019).

The fossil variety of the CY assemblage became less diverse, and the numbers of lycophytic spores of *Lundbladispora* and *Aratrisporites* increased sharply. This resembles the terrestrial plants distribution of the PTME interval in many areas of the world (Benton and Newell, 2014; Yu et al., 2015; Liu et al., 2020). This assemblage corresponds to the *Aratrisporites-Lundbladispora* assemblage proposed by Ouyang (1982), and Mesozoic plants become prominent (Ouyang, 1982). In northern China, the abundant occurrence of *Lundbladispora* corresponds to the *Lundbladispora-Cycadopites-Taeniaesporites* assemblage, however, *Aratrisporites* were not observed (Ouyang and Hou, 1999). The appearance of abundant cavate trilete spores can be traced back to the *Lundbladispora brevicula-Densoisporites nejburgii* assemblage in southern Tibet (Liu et al., 2020), and the *Protohaploxypinus microcorpus* zone plus the *Lunatisporites pellucidus* zone in eastern Australia (Fig.8).

In the lower part of the Kayitou Formation where the RF assemblage was developed, the palynofacies change sharply, and gymnosperm pollen became dominant. This appearance represents the gradual arrival of arid paleoclimates, and terrestrial vegetation entering the Mesozoic era (Fig. 8). This interval can be interpreted as an early recovery phase in the Early Triassic. The sharp rebounding of the species diversity in the Triassic was well demonstrated by palynological data from east Greenland (Hochuli et al., 2016), southern Tibet (Liu et al., 2020), the Sydney Basin in Australia (Vajda et al., 2020), and the Salt and Surghar Ranges in Pakistan (Schneebeli-Hermann and Bucher, 2015). Therefore, according to the correlation analysis of sporopollen assemblages, the CY assemblage represents the extinction stage, and the RF assemblage represents the recovery stage of the early Triassic after the extinction. However, the stratigraphic age of this turnover is not uniform in different regions, so these correlations are tentative.

5.2. Floral responses to the Permian–Triassic mass extinction

An accurate time frame is essential for studying floral responses to the Permian–Triassic mass extinction. South China, the most intensively studied region for PTME events, has several precise volcanic ash ages in both marine and terrestrial sections (Shen S Z et al., 2011; Wu Q, 2020). The main phase of marine extinctions in south China spans the conodont *Clarkina meishanensis* Zone to *Isarcicella isarcica* Zone and corresponds to Beds 25–28 at the GSSP Meishan section (Shen S Z et al., 2011; Burgess et al., 2014; Shen S Z et al., 2019). The time frame of the extinction was calibrated within 61±48ky, or even shorter (Li et al., 2016; Burgess et al., 2017; Shen S Z et al., 2019). In contrast, due to the lateral facies variability of terrestrial strata, the position of the PTB and extinction interval in terrestrial sections are still controversial in southwestern China (Zhang et al., 2016; Chu et al., 2020). According to the Stratigraphic Chart of China (2014), the Kayitou Formation is generally classified as the Early Triassic. The latest zircon age data also constrain the PTB to near the lower part of the Kayitou Formation, but the position is still indeterminate (Wu, 2020) (Fig 1).

The observations of palynology and paleobotany showed that the destruction of the *Gigantopteris*-dominated peat ecosystems occurred in the bottom part of the Kayitou Formation (Ouyang, 1982; Peng et al., 2006; Yu et al., 2015). The coal seams disappeared and the diversity of macrofossils decreased rapidly in the Kayitou Formation. In addition, many Mesozoic plants had their first appearances, and the plant assemblages transitioned into the *Annalepis-Peltaspermum* assemblage (Yu et al., 2015; Xu et al., 2022) which is equivalent to the CY assemblage in this study. From the floral perspective, the position of floral turnover occurred in the lower part of the Kayitou Formation, within a very narrow stratigraphic interval in southwestern China. However, the plant macrofossil data are inadequate to obtain a complete understanding on how the land plants responded to the PTME. Furthermore, plant macrofossils are subjected to considerable taphonomic filtering that can affect the interpretations made from them (e.g., DiMichele et el., 2020; Xu et al., 2022).

Previous palynological research showed that the spore and pollen diversity decreased sharply after the last coal bed (Ouyang, 1982; Peng et al., 2006; Yu et al., 2016; Zhang et al., 2016; Feng et al., 2020). This interval of sharp decrease in sporopollen was considered as the onset of forest extinction (Fig. 9) (Chu et al., 2019). However, the interval of the land plant extinction was not as short as the macrofossils suggests. Moderately common plant fossils continued to be present in the lower part of the Kayitou Formation in the Guanbachong section (Zhang et al., 2016; Xu et al., 2022), as well as in the sections investigated in this study. The low diversity populations immediately occurred following the disappearance of the *Gigantopteris*-dominated rainforest ecosystems in the Mide and Lengqinggou sections in southwestern China (Feng et al., 2020; Xu et al.,2022). The response of plants to the extinction is also shown in the CY assemblage of the bottom part of the Kayitou

Formation. Notably, the study of the overlying strata showed the abundance and diversity of pollen rebounding (Fig. 9). Gymnosperm pollen dominated the RF assemblage in the lower part of the Kayitou Formation, with the palyno-assemblage rich in *Alisporites*, *Protopinus* and *Pityosporites*. The gymnosperm pollen is interpreted as being mostly derived from an upland source, rather than from the lowland mire-forming vegetation (Xu et al., 2022; Wheeler et al., 2022). Increasing drought in the Early Triassic is often considered as a significant threat to plant survival (Benton and Newell, 2014). These upland plants were generally well adapted to survive in conditions of water shortage (Benton and Newell, 2014) and were likely drought-tolerant (DiMichele et al., 2020). Therefore, drought-tolerant plants growing in uplands were likely the first plants to recover after extinction as they were pre-adapted to the ensuing environmental conditions (e.g., Xu et al., 2022). In southwestern China, herbaceous lycophytes survived in coastal regions (Yu et al., 2010, 2015; Feng et al., 2020), and gymnosperms coniferopsida survived on uplands through the Permian-Triassic transition (Fig 10). Our new data further refines the understanding of vegetational changes during the aftermath of the PTME catastrophe in southwestern China. From the perspective of sporopollen studies, the extinction interval of the plants spans the lower part of the Kayitou Formation in southwestern China.

Subsequently, in the upper part of the Kayitou Formation and the Dongchuan Formation, the lithologies gradually change to red-colored siliciclastic rocks, which indicates an extremely arid paleoclimate (Zhang et al., 2016). This reddish lithology is widely distributed in non-marine strata in southwestern China and has almost no spore-pollen fossils, presumably due to taphonomic oxidization of organic materials including palynomorphs and their loss in post-deposition, rather than no plants present at this time (DiMichele et al., 2020; Xu et al., 2022). Although the main pulse of extinction did not completely eradicate the land plant systems, with the intensification of drought in the Triassic, macro and microfossil evidence of terrestrial vegetation disappeared completely in southwestern China. This phenomenon may be interpreted to represent the complete collapse of the land plant communities in lowland settings during this interval. These findings contrast with the hypothesis of the short and sudden extinction of marine life in the PTME, and supports the hypothesis that the extinction of terrestrial vegetation was a long-term and two-staged process in southwestern China.

However, the apparent response of terrestrial vegetation in different regions to the PTME event varies. Increasing evidence supports that the onset of the terrestrial crisis was earlier than the main marine extinction (Fielding et al., 2019; Chu et al., 2020; Wignall et al., 2020; Guo et al., 2022). In northern China, the paleoclimates gradually became more arid as early as the Wuchiapingian Stage when the peat swamps regionally disappeared (Wu et al., 2021), and the plant assemblages changed into a more arid-tolerant Euramerian-type flora (Broutin et al., 2020). The terrestrial ecological crisis in northern China occurred at a time some 270 ± 150 kyrs before the main marine extinction (Wignall et al., 2020; Dal Corso et al., 2022; Guo et al., 2022). In southern Tibet, the PTME only resulted in a short-term disturbance and range contraction of land-plant communities, and the terrestrial vegetation recovered after thousands of years (Liu et al., 2020). In the Sydney Basin, the collapse of *Glossopteris* flora occurred prior to 252.3 Ma (Fielding et al., 2019). Overall, the damage of the PTME event on the terrestrial vegetation is reliably supported, however, the response was closely related to the regional paleoclimates and types of plant species and genera present.

5.3. Likely lethal factors for the vegetation catastrophe during the PTME

Numerous mechanisms have been considered to have caused or contributed to the floral changes during the PTME, including extreme warming, aridity, acid rain, and wildfires (Benton and Newell, 2014; Dal Corso et al. 2022). However, the response of plants in different regions to the PTME varies, and not all environmental crises are reflected in southwestern China. Therefore, the actual mechanisms causing floral change should be discussed in detail.

The CO_2 released by the eruption of the Siberian Traps caused global warming (Burgess et al., 2017), and these elevated temperatures were once considered the primary lethal mechanism during the Permian–Triassic mass extinction (Benton, 2018). In southern China, the conodont apatite oxygen isotope record suggests a sharp increase in seawater temperature (Chen et al., 2013; Wang et al., 2020a). Clearly the increase in global temperature also existed in southern China. Biogeographic studies indicate that the environmental temperature changes have affected many plants' survival (Harley, 2011). In particular, for the C3 plants, photorespiration replaces photosynthesis at high temperatures and few plant species can survive in air temperature above 40 °C (Yamori et al., 2014). However, the effects of hyperthermia on paleo-flora are hard to predict, and how high the air temperature required to cause species extinction levels is unclear (Benton and Newell, 2014). Furthermore, aridity resulting from high temperatures was believed to be one of the PTME lethal factors on land (Benton, 2018; Wignall et al., 2020; Wang and Visscher, 2021; Dal Corso et al., 2022). The global terrestrial red beds in the Early Triassic directly reflects arid paleoclimates in the post-PTME period (Tabor et al., 2011). The appearance of *Lystrosaurus* and the increase of gymnosperms in the Early Triassic indicates the onset of drought conditions (Zhu et al., 2020). Most researchers acknowledged that increasing aridity was one of the important factors in plant community collapse (Benton and Newell, 2014). However, spores still dominated in the CY assemblages in the bottom part of the Kayitou Formation, and the high values of the chemical index of alteration (CIA) indicated that humid and hot environments persisted during the PTME in South China (Cao et al., 2019). The arid paleoclimates appeared later during the Dongchuan Formation. Evidently, aridity was possibly a factor of long-term terrestrial ecology disturbance during the Early Triassic in southwestern China.

On land, acid rain damaged forests and soils, and even today, acid rain is still a factor in vegetation destruction (Fenn et al., 2006; Dietze and Moorcroft 2011). Previous studies have modelled the massive acidic gas emissions from the Siberian Traps eruption, which generated intervals of highly acidic rain (Black et al., 2014; Sephton et al., 2015; Li et al., 2022). Acid rain could have posed a huge potential threat to the Late Permian terrestrial plants, and could cause the destruction of vegetation in a short time. Recent research suggested that explosive volcanism in southern China possessed the potential for a massive release of SO_2 over a short interval (Zhang et al., 2021). However, the time of the massive release of SO_2 from felsic volcanism in southern China occurred after the deforestation (Zhang et al., 2021). Therefore, the acid rain in southern China could have been an important factor delaying the local recovery of land plants. Fire is also a key ecosystem driver throughout geological time (Glasspool et al., 2015). The evidence for extensive wildfires in the PTME interval have been widely reported (Shao et al., 2012; Sun et al., 2017; Yan et al., 2019; Vajda et al., 2020; Lu et al., 2020; Cai et al., 2021). The abundant charcoal in mudstones and increasing amounts of inertinite in coal showed that the fire activity and intensity increased towards the PTME (Zhang et al., 2016; Yan et al., 2019; Cai et al., 2021). Furthermore, high atmospheric oxygen concentration (pO_2) supported the spread of wildfires (Glasspool and Scott, 2010). Wildfires are regarded to be closely linked to the evolution of the terrestrial ecology in southern China from the Late Permian to the Early Triassic.

The release of halogens and halocarbon compounds from the volcanic activity during the PTME period caused ozone depletion, which increased ultraviolet B-rays (UVB) radiation (Black et al., 2014). The high abundance of teratological sporomorphs during the PTME was generally attributed to increasing UVB radiation (Benca et al., 2018). Although this UVB radiation cannot directly kill plants, it could decrease the fertility of plants and thereby cause the collapse of forest systems (Dal Corso et al., 2022). In southern China, teratological spores and pollen are widespread across the Permian–Triassic transition (Chu et al., 2021). However, Chu et al. (2021) suggested that the mutagenesis was likely caused by metal toxicity, linked to increased Hg and Cu loading. Therefore, the UVB radiation effects in southern China is still debated.

A single lethal factor is unlikely to be responsible for all the changes and impacts seen in terrestrial ecosystems. The final extinction of vegetation in southwestern China would more likely be the result of a combination of different factors. The most probable scenario could be that the Siberian Traps eruptions released large amounts of toxic and harmful substances that destroyed the *Gigantopteris*-dominated rainforest ecosystems in short-term processes (Fig 10). Although gymnosperms rebounded after this, increasing drought caused by high temperatures and acid rain caused by regional volcanism inhibited plant recovery in the Early Triassic (Fig 10). Wildfire played an important role in both the initial destruction and the subsequent inhibition of plant recovery (Fig 10).

6. Conclusions

The palynological investigation of three borehole sections spanning through the entire Lopingian (the Late Permian) and the Permian–Triassic transitional strata in southwestern China, together with a recently updated radiogenic age, enables further evaluation of paleo-vegetation dynamics.

1. According to the vertical distribution of the palynological species and CONISS cluster analysis on the relative abundance of various palynomorph taxa in each sample, four palynomorph assemblages are subdivided, including the *Tripartites cristatus* var. *minor* - *Torispora laevigata* (ML) assemblage and the *Crassispora orientalis* - *Anticapipollis tornatilis* (OT) assemblage in the Xuanwei Formation, and the *Lundbladispora communis* - *Aratrisporites yunnanensis* (CY) assemblage and *Pteruchipollenites reticorpus* - *Protopinus fuyuanensis* (RF) assemblage in the overlying Kayitou Formation. From the perspective of sporopollen studies, the extinction interval of the plants spans the lower part of the Kayitou Formation in southwestern China.

2. Our new data further refines the understanding of vegetational changes during the aftermath of the PTME catastrophe in southwestern China. The PTME event induced a sharp decrease in plant diversity and change in vegetation-community composition. Subsequently, the upland gymnosperm abundance increased and dominated. These drought-tolerant plants growing in uplands were likely the first plants to recover after the extinction event in southwestern China. The macro and microfossil evidence of terrestrial vegetation disappeared completely in the upper part of the Kayitou Formation and the Dongchuan Formation. These findings support the

hypothesis that the extinction of terrestrial vegetation was a long-term and two-staged process in southwestern China.

3. The complete disappearance of vegetation could be attributed to short-term acid rain and high temperatures caused by volcanic activity, as well as the long-term wildfires and increasing aridity.

Acknowledgements

We thank Jason Hilton (University of Birmingham) for comments and revisions to the manuscript. This study is supported by the National Natural Science Foundation of China (Grant No. 41572090), the Fundamental Research Funds for the Central Universities, and the Yueqi Scholar fund of China University of Mining and Technology (Beijing).

Reference

Benca, J. P., Duijnstee, I. A. P. & Looy, C. V., 2018, UV- B–induced forest sterility: implications of ozone shield failure in Earth’s largest extinction. Science. Advances. 4, e1700618.

Benton, M. J., 2018, Hyperthermal-driven mass extinctions: killing models during the Permian-Triassic mass extinction: Philos Trans A Math Phys Eng Sci, v. 376, no. 2130.

Benton, M. J., and Newell, A. J., 2014, Impacts of global warming on Permo-Triassic terrestrial ecosystems: Gondwana Research, v. 25, no. 4, p. 1308-1337.

Bercovici, A., Cui, Y., Forel, M.B., Yu, J.X., and Vajda, V., 2015, Terrestrial paleoenvironment characterization across the Permian–Triassic boundary in South China: Journal of Asian Earth Sciences, v. 98, p. 225-246, https://doi.org/10.1016/j.jseaes.2014.11.016.

Berner R A, 2002. Examination of hypotheses for the Permo - Triassic boundary extinction by carbon cycle modeling. Proceedings of the National Academy of Sciences. 99(7):4172-4177. https://doi.org/10.1073/pnas.032095199

Black, B. A., Lamarque, J.-F., Shields, C. A., Elkins-Tanton, L. T., and Kiehl, J. T., 2014, Acid rain and ozone depletion from pulsed Siberian Traps magmatism: Geology, v. 42, no. 1, p. 67-70.

Broutin, J., Yu, J.X., Shi, X., Shu, W.C., and Qing, X., 2020, Terrestrial palaeofloral succession across the Permian–Triassic Boundary in the North and South China blocks: a brief review: PalZ, v. 94, no. 4, p. 633-644. https://doi.org/10.1007/s12542-020-00511-0

Burgess S.D, Bowring, S.A., Shen, S.Z., 2014, High-precision timeline for Earth's most severe extinction: Proceedings of the National Academy of Sciences, 111(9): 3316-3321. https://doi.org/10.1073/pnas.1317692111.

Burgess, S. D., Muirhead, J. D., and Bowring, S. A., 2017, Initial pulse of Siberian Traps sills as the trigger of the end-Permian mass extinction: Nature Communication, v. 8, no. 1, p. 164.

Cai, Y.f., Zhang, H., Feng, Z., and Shen, S.Z., 2021, Intensive Wildfire Associated With Volcanism Promoted the Vegetation Changeover in Southwest China During the Permian−Triassic Transition: Frontiers in Earth Science, v. 9. https://doi.org/10.3389/feart.2021.615841

Cao, Y., Song, H.Y., Algeo, T. J., Chu, D.L., Du, Y., Tian, L., Wang, Y.H., and Tong, J.N., 2019, Intensified chemical weathering during the Permian-Triassic transition recorded in terrestrial and marine successions: Palaeogeography, Palaeoclimatology, Palaeoecology, v. 519, p. 166-177. https://doi.org/10.1016/j.palaeo.2018.06.012

Cascales-Miñana, , B., and Cleal, C. J., 2013, The plant fossil record reflects just two great extinction events. Terra Nova, v. 26, No. 3, 195–200. https://doi.org/10.1111/ter.12086

Chen, B., Joachimski, M. M., Shen, S.Z., Lambert, L. L., Lai, X.L., Wang, X.D., Chen, J., and Yuan, D.X., 2013, Permian ice volume and palaeoclimate history: Oxygen isotope proxies revisited: Gondwana Research, v. 24, no. 1, p. 77–89.

Chu, D.L., Grasby, S. E., Song, H., Corso, J. D., Wang, Y., Mather, T. A., Wu, Y., Song, H., Shu, W., Tong, J., and Wignall, P. B., 2020, Ecological disturbance in tropical peatlands prior to marine Permian-Triassic mass extinction: Geology, v. 48, no. 3, p. 288-292.

Chu, D.L., Yu, J.X., Tong, J.N., Benton, M. J., Song, H.J., Huang, Y.F, Song, T., and Tian, L., 2016, Biostratigraphic correlation and mass extinction during the Permian-Triassic transition in terrestrial-marine siliciclastic settings of South China: Global and Planetary Change, v. 146, p. 67–88. https://doi.org/10.1016/j.gloplacha.2016.09.009

Cui, Y., Bercovici, A., Yu, J.X., Kump, L. R., Freeman, K. H., Su, S.G., and Vajda, V., 2017, Carbon cycle perturbation expressed in terrestrial Permian–Triassic boundary sections in South China: Global and Planetary Change, v. 148, p. 272–285. https://doi.org/10.1016/j.gloplacha.2015.10.018

Dal Corso, J., Song, H.J., Callegaro, S., Chu, D.L., Sun, Y.D., Hilton, J., Grasby, S. E., Joachimski, M. M., and Wignall, P. B., 2022, Environmental crises at the Permian–Triassic mass extinction: Nature Reviews Earth & Environment.

DiMichele, W.A., Bashforth, A.R., Falcon-Lang, H.J., Lucas, S.G., 2020. Uplands, lowlands, and climate: taphonomic megabiases and the apparent rise of xeromorphic, drought-tolerant flora during the Pennsylvanian–Permian transition. Palaeogeogr. Palaeoclimatol. Palaeoecol. 559, 109965 https://doi.org/10.1016/j. palaeo.2020.109965.

Domeier, M., and Torsvik, T. H., 2014, Plate tectonics in the late Paleozoic: Geoscience Frontiers, v. 5, no. 3, p. 303–350.

Feng, Z., Wei, H.B., Guo, Y., He, X.Y., Sui, Q., Zhou, Y., Liu, H.Y., Gou, X.D., and Lv, Y., 2020, From rainforest to herbland: New insights into land plant responses to the end-Permian mass extinction: Earth-Science Reviews, v. 204, 103153 https://doi.org/10.1016/j.earscirev.2020.103153

Fielding, C. R., Frank, T. D., McLoughlin, S., Vajda, V., Mays, C., Tevyaw, A. P., Winguth, A., Winguth, C., Nicoll, R. S., Bocking, M., and Crowley, J. L., 2019, Age and pattern of the southern high-latitude continental end-Permian extinction constrained by multiproxy analysis: Nat Commun, v. 10, no. 1, p. 385.

Glasspool, I. J., and Scott, A. C., 2010, Phanerozoic concentrations of atmospheric oxygen reconstructed from sedimentary charcoal: Nature Geoscience, v. 3, no. 9, p. 627–630.

Glasspool, I. J., Scott, A. C., Waltham, D., Pronina, N., and Shao, L., 2015, The impact of fire on the Late Paleozoic Earth system: Frontiers in Plant Science, v. 6, 756. 10.3389/fpls.2015.00756

Guo, W.W., Tong, J.N., He, Q., Hounslow, M. W., Song, H.Y., Dal Corso, J., Wignall, P. B., Ramezani, J., Tian, L., and Chu, D.L., 2022, Late Permian–Middle Triassic magnetostratigraphy in North China and its implications for terrestrial-marine correlations: Earth and Planetary Science Letters, v. 585, 117519. https://doi.org/10.1016/j.epsl.2022.117519

Harley, C. D., 2011, Climate change, keystone predation, and biodiversity loss: Science, v. 334, no. 6059, p. 1124-1127.

He, B., Zhong, Y.T., Xu, Y.G, and Li, X.H., 2014, Triggers of Permo-Triassic boundary mass extinction in South China: The Siberian Traps or Paleo-Tethys ignimbrite flare-up?. Lithos, 204, 258-267. https://doi.org/10.1016/j.lithos. 2014. 05.011.

Hochuli, P.A., Hermann, E., Vigran, J.O., Bucher, H., Weissert, H., 2010a. Rapid demise and recovery of plant ecosystems across the end-Permian extinction event. Global Planet Chang. 74 (3–4), 144–155.

Hochuli, P.A., Sanson-Barrera, A., Schneebeli-Hermann, E., Bucher, H., 2016. Severest crisis overlooked—worst disruption of terrestrial environments postdates the Permian–Triassic mass extinction. Sci. Rep. 6, 28372.

Huang, B.C., Yan, Y.G., Piper John D. A., Zhang, D.H., Yi, Z.Y., Yu S., Zhou, T.H., 2018, Paleomagnetic constraints on the paleogeography of the East Asian blocks during Late Paleozoic and Early Mesozoic times. Earth-Science Reviews, 186:8–36. https://doi.org/10.1016/j.earscirev.2018.02.004.

Li, M.H., Frank, T. D., Xu, Y.L., Fielding, C. R., Gong, Y.Z., and Shen, Y.A., 2022, Sulfur isotopes link atmospheric sulfate aerosols from the Siberian Traps outgassing to the end-Permian extinction on land: Earth and Planetary Science Letters, v. 592.

Li, M.S., Ogg, J., Zhang, Y., Huang, C.J., Hinnov, L., Chen, Z.Q., and Zou, Z.Y., 2016, Astronomical tuning of the end-Permian extinction and the Early Triassic Epoch of South China and Germany: Earth and Planetary Science Letters, v. 441, p. 10–25. https://doi.org/10.1016/j.epsl.2016.02.017

Liu, F., Peng, H.P., Bomfleur, B., Kerp, H., Zhu, H.C., and Shen, S.Z., 2020, Palynology and vegetation dynamics across the Permian–Triassic boundary in southern Tibet: Earth-Science Reviews, v. 209, 103278. https://doi.org/10.1016/j.earscirev.2020.103278

Lu, J., Wang, Y., Yang, M.F., Zhang, P.X., Bond, D. P. G., Shao, L.Y., and Hilton, J., 2022, Diachronous end-Permian terrestrial ecosystem collapse with its origin in wildfires: Palaeogeography, Palaeoclimatology, Palaeoecology, v. 594, 110960. https://doi.org/10.1016/j.palaeo.2022.110960

Lu, J., Zhang, P.X., Yang, M.F., Shao, L.Y., and Hilton, J., 2020, Continental records of organic carbon isotopic composition (δ13Corg), weathering, paleoclimate and wildfire linked to the End-Permian Mass Extinction: Chemical Geology, v. 558.

Nowak, H., Schneebeli-Hermann, E., and Kustatscher, E., 2019, No mass extinction for land plants at the Permian-Triassic transition: Nat Commun, v. 10, no. 1, p. 384.

Ouyang, S., 1982, Upper Permian and Lower Triassic palynomorphs from eastern Yunnan, China: Canadian Journal of Earth Sciences, v. 19, no. 1, p. 68–80.

Peng, Y.Q., Yu, J.X., Gao, Y.Q., and Yang, F.Q., 2006, Palynological assemblages of non-marine rocks at the Permian–Triassic boundary, western Guizhou and eastern Yunnan, South China: Journal of Asian Earth Sciences, v. 28, no. 4–6, p. 291–305. https://doi.org/10.1016/j.jseaes.2005.10.007

Rampino, M. R., and Eshet, Y., 2018, The fungal and acritarch events as time markers for the latest Permian mass extinction: An update: Geoscience Frontiers, v. 9, no. 1, p. 147–154.

Rees, P. M., 2002, Land-plant diversity and the end-Permian mass extinction: Geology, v. 30, no. 9, p. 827–830.

Retallack, G.J., Veevers, J.J., Morante, R., 1996. Global coal gap between Permian–Triassic extinction and Middle Triassic recovery of peat-forming plants. GSA Bulletin. 108, 195–207

Schmitz, M. D., and Kuiper, K. F., 2013, High-Precision Geochronology: Elements, v. 9, no. 1, p. 25–30.

Schneebeli-Hermann, E., Bucher, H., 2015. Palynostratigraphy at the Permian-Triassic boundary of the Amb section, Salt Range, Pakistan. Palynology 39 (1), 1–18.

Sephton, M. A., Jiao, D., Engel, M. H., Looy, C. V., and Visscher, H., 2015, Terrestrial acidification during the end-Permian biosphere crisis?: Geology, v. 43, no. 2, p. 159–162.

Shao, L.Y., Hao W., Xiaohui, Y., Jing, L., and Mingquan, Z., 2012, Paleo-fires and atmospheric oxygen levels in the latest Permian: Evidence from maceral compositions of coals in eastern Yunnan, southern China: Acta Geologica Sinica-English Edition, v. 86, no. 4, p. 949–962.

Shao, L.Y., Liu, H.M., Tian, B.L., Zhang, P.F., 1998, Sedimentary evolution and its controls on coal accumulation for the Late Permian in the Upper Yangtze area: Acta sedimentologica sinica, v. 16, no. 2, p. 55–60 (in Chinese with English abstract).

Shao, L.Y., Gao, C.X., Zhang, C., Wang, H., Guo, L.J., Gao, C.H., 2013, Sequence-Palaeogeography and coal accumulation of Late Permian in Southwestern China: Acta sedimentological sinica, v. 31, no. 5, p. 856–866 (in Chinese with English abstract).

Shao, L.Y, Wang, X.T, Wang, D., Li, M., Wang, S., Li, Y., Shao, K., Zhang, C., Gao, C., Dong, D., Cheng, A., Lu, J., Ji, C., and Gao, D., 2020, Sequence stratigraphy, paleogeography, and coal accumulation regularity of major coal-accumulating periods in China: International Journal of Coal Science & Technology, v. 7, no. 2, p. 240–262.

Shen, S.Z., Ramezani, J., Chen, J., Cao, C.Q., Erwine, D.H., Zhang, H., Xiang, L., Erwin, D.H., Henderson, C.M., Zhen, F.Q., Bowring, S.A., Wang, Y., Li, X.H., Wang, X.D., Yuan, D.X., Zhang, Y.C., Mu, L., and Wu, Y.S., 2019, A sudden end-Permian mass extinction in South China: GSA Bulletin, v. 131, p. 205-223, https://doi.org/10.1130/B31909.1.

Shen, S. Z., Crowley, J. L., Wang, Y., Bowring, S. A., Erwin, D. H., Sadler, P. M., Cao, C. Q., Rothman, D. H., Henderson, C. M., Ramezani, J., Zhang, H., Shen, Y., Wang, X. D., Wang, W., Mu, L., Li, W. Z., Tang, Y. G., Liu, X. L., Liu, L. J., Zeng, Y., Jiang, Y. F., and Jin, Y. G., 2011, Calibrating the end-Permian mass extinction: Science, v. 334, no. 6061, p. 1367–1372.

Spina, A., Cirilli, S., Utting, J., and Jansonius, J., 2015, Palynology of the Permian and Triassic of the Tesero and Bulla sections (Western Dolomites, Italy) and consideration about the enigmatic species Reduviasporonites chalastus: Review of Palaeobotany and Palynology, v. 218, p. 3-14.

Sun, Y.Z., Zhao, C.L., Püttmann, W., Kalkreuth, W., and Qin, S.J., 2017, Evidence of widespread wildfires in a coal seam from the middle Permian of the North China Basin: Lithosphere, v. 9, no. 4, p. 596–608. https://doi.org/10.1130/L638.1

Tabor, N. J., Smith, R. M. H., Steyer, J. S., Sidor, C. A., and Poulsen, C. J., 2011, The Permian Moradi Formation of northern Niger: Paleosol morphology, petrography and mineralogy: Palaeogeography, Palaeoclimatology, Palaeoecology, v. 299, no. 1-2, p. 200–213.

Vajda, V., McLoughlin, S., Mays, C., Frank, T. D., Fielding, C. R., Tevyaw, A., Lehsten, V., Bocking, M., and Nicoll, R. S., 2020, End-Permian (252 Mya) deforestation, wildfires and flooding—An ancient biotic crisis with lessons for the present: Earth and Planetary Science Letters, v. 529, 115875. https://doi.org/10.1016/j.epsl.2019.115875

Wang, C.J., and Visscher, H., 2021, A molecular biomarker for end-Permian plant extinction in South China: Geology, v. 49, no. 12, p. 1489–1494. https://doi.org/10.1130/G49123.1

Wang, J., Shao, L.Y., Wang, H., Spiro, B., and Large, D., 2018, SHRIMP zircon U–Pb ages from coal beds across the Permian–Triassic boundary, eastern Yunnan, southwestern China: Journal of Palaeogeography, v. 7, no. 2, p. 117–129.

Wang, W.Q., Garbelli, C., Zhang, F.F., Zheng, Q.F., Zhang, Y.C., Yuan, D.X., Shi, Y.K., Chen, B., and Shen, S.Z., 2020a, A high-resolution Middle to Late Permian paleotemperature curve reconstructed using oxygen isotopes of well-preserved brachiopod shells: Earth and Planetary Science Letters, v. 540.

Wang, X.T., Shao, L.Y., Eriksson, K.A., Yan, Z.M., Wang, J.M., Li, H., Zhou, R.X., and Lu, J., 2020b, Evolution of a plume-influenced source-to-sink system: An example from the coupled central Emeishan large igneous province and adjacent western Yangtze cratonic basin in the Late Permian, SW China: Earth-Science Reviews, v. 207, 103224, https://doi.org/10.1016/j.earscirev.2020.103224.

Wang, Z.Q. 1989. Permian gigantic palaeobotanical events in North China. Acta Palaeontologica Sinica 28(3): 314–337. (in Chinese with English abstract).

Wignall, P., Chu, D.L., Hilton, J., Dal Corso, J., Wu, Y.Y., Wang, Y., Atkinson, J., Tong, J.N. 2020. Death in the Shallows: the record of Permo-Triassic mass extinction in paralic settings, southwest China. Global and Planetary Change 189: 193176 https://doi.org/10.1016/j.gloplacha.2020.103176

Wood, G.D., Gabriel, A.M., Lawson, J.C., 1996. In: Jansonius, J., McGregor, D.C. (Eds.), Palynological Techniques Processing and Microscopy. Palynology: Principles and Applications. Publishers Press, Salt Lake City, Utah, pp. 29–50.

Wu, Q., 2020, High-precision zircon U-Pb geochronological studies of the Permian ash beds from China and North America: University of Science and Technology of China. (in Chinese with English abstract)

Xiong, C., and Wang, Q., 2016, Permian–Triassic land-plant diversity in South China: Was there a mass extinction at the Permian/Triassic boundary?. Paleobiology, v. 37, no. 1, p. 157–167.

Xu, Z., Hilton, J., Yu. J.X., Wignall, P.B., Yin, H.F., Xue, Q., Ran, W.J., Hui, L., Shen, J., Meng, F.S. 2022. Mid-Permian to Late Triassic plant species richness and abundance patterns in South China: Co-evolution of plants and the environment through the Permian-Triassic transition. Earth-Science Reviews 232: 104136 https://doi.org/10.1016/j.earscirev.2022.104136

Yamori, W., Hikosaka, K., and Way, D. A., 2014, Temperature response of photosynthesis in C3, C4, and CAM plants: temperature acclimation and temperature adaptation: Photosynth Res, v. 119, no. 1–2, p. 101–117.

Yan, Z.M., Shao, L.Y., Glasspool, I.J., Wang, X.T., and Wang, H., 2019, Frequent and intense fires in the final coals of the Paleozoic indicate elevated atmospheric oxygen levels at the onset of the end-Permian mass extinction event: International Journal of Coal Geology, v. 207, p. 75-83, https://doi.org/10.1016/j.coal.2019.03.016.

Yu, J.X., Broutin, J., Chen, Z.Q., Shi, X., Li, H., Chu, D.L., and Huang, Q.S., 2015, Vegetation changeover across the Permian–Triassic Boundary in Southwest China: Extinction, survival, recovery and palaeoclimate: A critical review: Earth-Science Reviews, v. 149, p. 203-224, https://doi.org/10.1016/j.earscirev.2015.04.005.

Yu, J.X., Broutin, J., Huang, Q.S., Grauvogel-Stamm, L., 2010. Annalepis, a pioneering lycopsid genus in the recovery of the Triassic land flora in South China. C. R. Palevol. 9, 479–486. https://doi.org/10.1016/j.crpv.2010.09.004.

Yuan, D.X., Shen, S.Z., Henderson, C. M., Chen, J., Zhang, H., and Feng, H.Z., 2014, Revised conodont-based integrated high-resolution timescale for the Changhsingian Stage and end-Permian extinction interval at the Meishan sections, South China: Lithos, v. 204, p. 220–245.

Zhang, H., Cao, C.Q., Liu, X.L., Mu, L., Zheng, Q.F., Liu, F., Xiang, L., Liu, L.J., and Shen, S.Z., 2016, The terrestrial end-Permian mass extinction in South China: Palaeogeography, Palaeoclimatology, Palaeoecology, v. 448, p. 108–124.

Zhang, H., Zhang, F.F., Chen, J.B., Erwin, D.H., Syverson, D.D., Ni, P., Rampino, M., Chi, Z., Cai, Y.F., Xiang, L., Li, W.Q., Liu, S.G., Wang, R.C., Wang, X.D., Feng, Z., Li, H.M., Zhang, T., Cai, H.M., Zheng, W., Cui, Y., Zhu, X.K., Hou, Z.Q., Wu, F.Y., Xu, Y.G., Planavsky, N., and Shen, S.Z., 2021, Felsic volcanism as a factor driving the end-Permian mass extinction: Science advances, v. 7, DOI: 10.1126/sciadv.abf8142

Zhu, Z.C., Kuang, H.W., Liu, Y.Q., Benton, M. J., Newell, A. J., Xu, H., An, W., Ji, S. A., Xu, S.C., Peng, N., Zhai, Q.G, and Dey, S., 2020, Intensifying aeolian activity following the end-Permian mass extinction: Evidence from the Late Permian–Early Triassic terrestrial sedimentary record of the Ordos Basin, North China: Sedimentology, v. 67, no. 5, p. 2691–-2720.

Supplementary material

Table S1 Statistical table of percentage content of main palynological species

Assemblages		Species (%)
the Early Triassic	M-L assemblage	*Stereisporites minimus* (0-0.63); *Leiotriletes pulvinulus* (0-0.59); *L. adnatus* (0-0.63); *L. sporadicus* (0-0.68); *L. cyathidites* (0-1.18); *L.* spp. (0.63-2.56); *Waltzispora strictura* (0-1.28); *W.* spp.(0-0.63); *Dictyophyllidites mortoni* (0-0.68); *D.* spp.(0-0.34); *C. pallida*(0-1.28); *C.* spp. (0-2.50); *Punctatisporites minutus* (0-1.18); *P. punctatus*(0-0.34); *P.* spp.(1.28-4.27); *G.* spp.(1.37); *C. micaceus*(1.18-5.14); *C. microgranus* (0-1.88); *C. pressus*(0-3.21); *C. orbicularis*(0-0.34); *C.* spp. (0.59-14.53); *C. mictus* (0-0.85); *V. microtuberosus*(0-0.68); *V*. spp. (1.18-2.05); *Acanthotriletes* spp.(0-0.64); *Apiculatasporites* spp. (0-1.25); *A*. spp. (0-1.71); *N*. spp. (0-1.25); *Baculatisporites* spp. (0-3.42); *Tripartites cristatus* var. *minor*(0-0.63); *Densosporites anulatus*(0-0.68); *D*.spp. (0-0.34); *Spinozonotriletes* spp. (0-0.59); *C. orientalis*(0-1.37); *Kraeuselisporites* spp. (1.18-3.42); *Lundbladispora communis*(0-0.68); *L*. spp. (0-1.28); *Torispora laevigata*(0-0.85); *T*. spp.(0-1.71); *P. minutus*(0-0.85); *A*. spp. (0-0.63); *Yunnanospora radiate*(0-0.34); *Vesicaspora* spp. (0-0.63); *Protohaploxypinus* spp.(0-5.89); *Gardenasporites firmus*(0-0.68); *G*. spp. (0-0.68); *Lueckisporites* spp. (0-0.34); Lunatisporites spp. (2.40-8.82); *Striatopodocarpites* spp. (0-1.18); *Alisporites fusiformis*(0-0.63); *A. auritus*(0-2.94); A. spp.(2.4-3.21); *Sulcatisporites* sp(0-0.68); *Protopinus fuyuanensis*(0-5.88); *P. asymmetricus*(0-3.53); *P. cyclocorpus*(0-3.53); *Platysaccus papilionis*(0-2.94); *P*. spp.(1.25-5.77); *Piceaepollenites* spp. (0-1.28); *Pteruchipollenites reticorpus*(1.71-8.90); *P. caytoniformis*(0-0.68); *Abietineaepollenites* spp.(1.28-4.71); *Klausipollenites* spp. (1.92-5.88); *Pityosporites* spp. (7.06-30.00); *Anticapipollis tornatilis*(0-5.98); *A. rectangularis*(0-0.85); *Disacciatrileti*(12.82-21.76); *Urmites* spp. (0-0.85); *Cycadopites* spp. (0-1.25)
	O-T assemblage	*L. adnatus*(0-1.2); *L. cyathidites*(0.2.99); *L. ornatus* (0-0.6); *L.* spp. (0-4.91); *Waltzispora strictura*(0-1.8); *W*. spp.(0-1.2); *Dictyophyllidites mortoni*(0-0.6); *D. discretus*(0-0.6); *Concavisporites* spp. (0-0.63); *C*. spp.(0-0.37); *Punctatisporites minutus*(0-1.58); *P*. spp.(0.32-1.59); *G*. spp. (0-2.39); *C. micaceus*(0-4.75); *C. microgranus*(0-0.95); *C. pressus*(0-0.63); *C*. spp.(0.37-4.75); *V*. spp. (0-0.37); *A*. spp.(0-1.2); *Lophotriletes mictus*(0-0.6); *L*. spp.(0.37-5.39); *A. tesotus*(0-1.12); *A*. spp. (0.8-3.73); *Raistrickia media*(0-0.32); *Neoraistrickia irregularis*(0-0.37); *N. spanis*(0-0.6); *N.* spp. (0-2.99); *Baculatisporites* spp. (0-0.32); *Tripartites cristatus* var. *minor*(0-4.79); *Lycospora* spp. (0-1.49); *Stenozonotriletes* spp. (0-0.37); *Densosporites anulatus*(0-0.63); *D. paranulatus*(0-0.63); *D*.spp. (0.4-0.75); *Propterisispora verruculifera*(0-1.8); *P. sparsus*(0-0.6); *P*. spp. (0-1.8); *Crassispora minuta*(0-2.24); *C. orientalis*(0-10.18); *C*. spp. (1.99-16.17); *Kraeuselisporites* spp. (0-2.61); *Wilsonisporites radiates*(0-0.37); Lundbladispora communis(1.8-20.52); *L. minima*(0-1.12); *L. subornata*(0.63-1.99); *L*. spp. (4.19-14.12); *Laevigatosporites minimus*(0-0.32); *L. vulgaris*(0-0.32); *P. minutus*(0-0.6); *Tuberculatosporites* spp.(0-0.37); *Striolatospora* spp. (0-2.99); *Aratrisporites minimus*(1.2-3.19); *A.*

		yunnanensis(8.21-16.73); *A*. spp. (8.98-26.87); *Yunnanospora radiate*(0-1.2) *Cordaitina* spp.(0-0.4); *Vesicaspora ooidea*(0-0.32); *Vesicaspora* spp. (0-1.59); *Protohaploxypinus* spp. (0-0.8); *G*. spp. (0-0.8); *Lueckisporites* spp. (0-0.4); *A. auritus*(0-0.32); *A*. spp. (0-0.75); *Protopinus fuyuanensis*(0-0.8); *P*. spp. (0-0.8); *Platysaccus papilioni*(0-0.32); *P.* spp. (0-0.63); *Piceaepollenites* spp. (0-0.32); *Pityosporites* spp.(0.37-18.99); *Anticapipollis tornatilis*(0-0.32); *Disacciatrileti*(0-0.32); *Cycadopites* spp. (0-0.32)
the Late Permian	CY assemblage	*Stereisporites minimus*(0-0.16); *Leiotriletes pulvinulus*(0-1.04); *L. adnatus*(0-3.15); *L. sporadicus*(0.36-5.45); *L. concavus*(0-1.54); *L. exiguous*(0-1.26); *L. cyathidites*(0-1.54); *L. ornatus*(0.1.54); *L.* spp. (0.77-11.55); *Retusotriletes* spp.(0-0.6); *Gulisporites cochlearius*(0-1.5); *G*. spp. (0-1.04); *Waltzispora strictura*(0-4.78); *W. yunnanensis*(0-0.36); *W*. spp. (0-1.59); *Dictyophyllidites mortoni*(0-2.45); *D. discretus*(0-0.98); *D*. spp. (0-3.92); *Concavisporites* spp.(0-1.54); *Calamospora pusilla*(0-0.59); *C. microrugosa*(0-3); *C. pallida*(0-0.47); *C*. spp. (0-2.96); *Punctatisporites minutus*(0-2.35); *P. elegans*(0-2.4); *P. distalis*(0-3.0); *P. palmipedites*(0-0.6); *P. latilus*(0-0.52); *P. punctatus*(0-0.9); *P*. spp. (0.36-14.71); *Granulatisporites mirus*(0-1.06); *G. adnatoides*(0-1.99); *G. brachytus*(0-0.79); *G*. spp. (0-3.15); Cyclogranisporites pressus(0-1.26); *C. micaceus*(0-2.36); *C. microgranus*(0-1.26); *C. labiatus*(0-0.69); *C. pressus*(0-0.36); *C. orbicularis*(0-0.3); *C.* spp.(0.53-5.35); *Lunzisporites* spp. (0-0.8); *Converrucosisporites capitatus*(0-0.47); *C. mictus*(0-0.31); *C. confractus*(0-0.79); *Verrucosisporites ovimammus*(0-1.88); *V. crassoides*(0-2.08); *V. pergranulus*(0-2.05); *V. microtuberosus*(0-3.64); *V. sinensis*(0-0.49); *V.* spp. (0-6.18); *Acanthotriletes* spp.(0-1.8); *Nixispora sinica*(0-1.32); *Apiculatasporites nanus*(0-1.37); *A. spinulistratus*(0-0.53); *A. spp.* (0-8.25); *Lophotriletes mictus*(0-0.4); *L. confertus*(0-0.4); *L*. spp. (0-3.98); *Apiculatasporites* spp.(0-0.26); *Apiculatisporis variocorneus*(0-0.53); *A. pyriformis*(0-0.53); *A. tesotus*(0-1.47); *A*. spp. (0-3.44); *Pustulatisporites* spp.(0-0.63); *Schopfites* sp(0-0.52); *Raistrickia media*(0-0.26); *R*. spp. (0-1.57); *Neoraistrickia irregularis*(0-3.44); *N. spanis*(0-1.03); *N. robusta*(0-1.54); *N. rigida*(0-3.44); *N*. spp. (0-1.42); *Mooreisporotes* sp.(0-1.06); *Baculatisporites* spp. (0-2.08); *Conbaculatisporites* spp.(0-0.36); *Convolutispora* spp.(0-0.6); *Foveosporites foratus*(0-0.69); *Reticulatisporites* spp.(0-0.52); *Triquitrites sinensis*(0-2.35); *T. attenuates*(0-2.37); *T. rugulatus*(0-3.51); *T*. spp. (0-1.89); *Tripartites cristatus* var. *minor*(0-10.55); *Lycospora* spp. (0-0.52); Stenozonotriletes spp.(0-0.18); *Densosporites anulatus*(0-0.69); *D. paranulatus*(0-0.3); *D*.spp. (0-2.1); *Simozonotriletes* spp. (0-0.59); *Spinozonotriletes* spp. (0-0.79); *Verrucingulatisporites* spp. (0-0.36); *Camarozonosporites* sp(0-0.3); *Propterisispora verruculifera*(0-11.98); *P. sparsus*(0-23.67); *P*. spp. (0-2.06); *Crassispora minuta*(0-7.9); *C. orientalis*(1.56-46.48); *C*. spp.(0-23.8); *Patellisporites meishanensis*(0-1.03); *Kraeuselisporites* spp. (0-2.31); *L. minima*(0.63-1.99); *L*. spp. (0-3.09); *Laevigatosporites minimus*(0.549-1.32); *L. lineolatus*(0-1.8); *L. vulgaris*(0-1.06); *L. maximus*(0-2.4); *L*. spp.(0.94-7.22); *Torispora laevigata*(0-1.18); *T. secures*(0-1.76); *T*. spp.(0-4.9); *Punctatosporites scabellus* (0-3.55); *P. minutus*(0-1.18); *P*. spp. (0-1.04); *Latosporites* sp.(0-1.44); *Tuberculatosporites* spp.(0-1.96); *Striolatospora* spp.(0-0.34); *A. yunnanensis*(0-0.52); *A*. spp. (0-3.85); *Yunnanospora radiate*(0-48.53)

		Cordaitina spp.(0-0.52); *Florinites pumicosus*(0-0.47); *F. florin*(0-0.26); *F.* spp. (0-1.54); *Vesicaspora ooidea*(0-1.06); *Vesicaspora* spp. (0-1.32); *Protohaploxypinus* spp. (0-1.72); *Gardenasporites firmus*(0-0.34); *Lueckisporites* spp. (0-1.03); *Striatopodocarpites* spp.(0-0.34); *A.* spp. (0-1.37); *P.* spp. (0-0.34); P. spp.(0-1.03); *Piceaepollenites* spp.(0-0.34); *Vitreisporites parvus*(0-0.53); *V. cryptocorpus*(0-0.26); *V.* sp.(0-0.53); *Klausipollenites* spp. (0-0.94); *Pityosporites* spp. (0-2.08); *Bactrosporites diptherus*(0-0.72); *B. ovatus*(0-0.53); *B.* spp.(0-1.54); *Anticapipollis tornatilis*(0-26.12); *A. rectangularis*(0-2.64); *A.* spp. (0-23.85); *Disacciatrileti*(0-4.12); *Urmites* spp. (0-1.18); *Cycadopites* spp.(0-1.04)
	RF assemblage	*Stereisporites minimus*(0-0.19); *Leiotriletes pulvinulus*(0-1.55); *L. adnatus*(1.68-5.9); *L. sporadicus*(0.21-1.55); *L. concavus*(0-1.86); *L. exiguous*(0-0.19); *L. ornatus*(0-0.21); *L.* spp. (1.65-4.04); *Gulisporites cochlearius*(0-0.19); *G.* spp.(0-0.19); *Waltzispora strictura*(0-0.41); *W. yunnanensis*(0-0.62); *W.* spp. (0-0.94); *Dictyophyllidites mortoni*(0-0.31); *Concavisporites* spp.(0-0.21); *Calamospora pusilla*(0-1.03); *C. microrugosa*(0.75-1.55); *C. pallida*(0-0.19); *C.* spp.(0.62-5.15); *Punctatisporites minutus*(0-0.93); *P. elegans*(0-0.75); *P. distalis*(0-0.19); *P.* spp. (0-1.88); *Granulatisporites mirus*(0-0.31); *G. adnatoides* (0.21-1.55); *G. brachytus*(0-0.41); *G.* spp. (0.21-1.13); *Cyclogranisporites pressus*(0.62-0.94); *C. micaceus*(0.31-1.51); *C. microgranus*(0-0.56); *C. pressus* (0-0.38); *C.* spp.(0.19-1.51); *Converrucosisporites capitatus*(0-0.21); *C. mictus*(0-0.41); *C. confractus*(0-0.62); *Verrucosisporites ovimammus*(0.21-0.93); *V. crassoides*(0-2.82); *V. pergranulus*(0.21-1.55); *V. microtuberosus*(0-1.88); *V. sinensis*(0-0.94); *V.* spp.(0.93-12.62); *Nixispora sinica*(0.37-3.77); *Apiculatasporites nanus*(0-0.19); *A. spinulistratus*(0-0.19); *A.* spp.(0-0.37); *Lophotriletes mictus*(0-0.62); *L. confertus*(0-0.31); *L.* spp. (0-0.56); *Apiculatisporis variocorneus*(0-1.03); *A. pyriformis*(0-0.21); *A. tesotus*(0-0.62); *A.* spp. (0-1.03); *Raistrickia media*(0-0.21); *R.* spp. (0-0.37); *Neoraistrickia irregularis*(0-0.21); *N. spanis*(0-0.82); *N. robusta*(0-0.19); *N.* spp. (0-0.62); *Mooreisporotes* sp(0-0.62); *Conbaculatisporites* spp. (0-0.93); *Convolutispora* spp. (0-0.62); *Foveosporites foratus*(0-0.31); *Reticulatisporites* spp. (0-0.21); *Triquitrites sinensis*(0-3.71); *T. attenuates*(0-1.03); *T. rugulatus*(0-0.41); *T.* spp. (0-2.48); *Tripartites cristatus* var. *minor*(8.21-30.75); *Lycospora* spp. (0-0.41); *Stenozonotriletes* spp. (0-0.62); *Densosporites anulatus*(0-0.93); *D. paranulatus*(0-0.31); *D.*spp. (0.21-0.75); *Simozonotriletes* spp. (0-0.38); *Verrucingulatisporites* spp. (0-0.62); *Camarozonosporites* sp(0-0.31); *Propterisispora verruculifera*(0.62-2.64); *P. sparsus*(0.62-18.47); *P.* spp. (0-0.94); *Crassispora minuta*(0-0.19); *C. orientalis*(0-1.31); *Kraeuselisporites* spp. (0-0.62); *Wilsonisporites radiates*(0-13.04); *L.* spp. (0-0.31); *Laevigatosporites minimus*(0.56-1.44); *L. lineolatus*(0-0.41); *L. vulgaris*(0-0.21); *L. maximus*(0-0.62); *Torispora laevigata*(0-8.87); *T. secures*(0-2.98); *T. verrucosa*(0-2.8); *T.* spp. (0.62-9.33); *Macrotorispora gigantean*(0-0.62); *Punctatosporites scabellus*(0.21-2.82); *P. minutus*(0-0.93); *P.* spp. (0.93-3.73); *Thymospora mesozoica*(0-0.62); *T.* spp. (1.12-11.19); *Tuberculatosporites* spp. (0-0.21); *Yunnanospora radiate*(0-6.03) *Cordaitina* spp.(0-0.19); *Florinites pumicosus*(0-0.19); *F. florin*(0-0.21); *F.* spp. (0-0.62); *Vesicaspora ooidea*(0-0.19); *Vesicaspora* spp. (0-0.41); Pityosporites spp. (0-0.21); *Anticapipollis tornatilis*(0-0.41); *A.* spp. (0-0.82); *Urmites* spp. (0.37-0.82); *Cycadopites* spp. (0.19-0.37)

Figure captions:

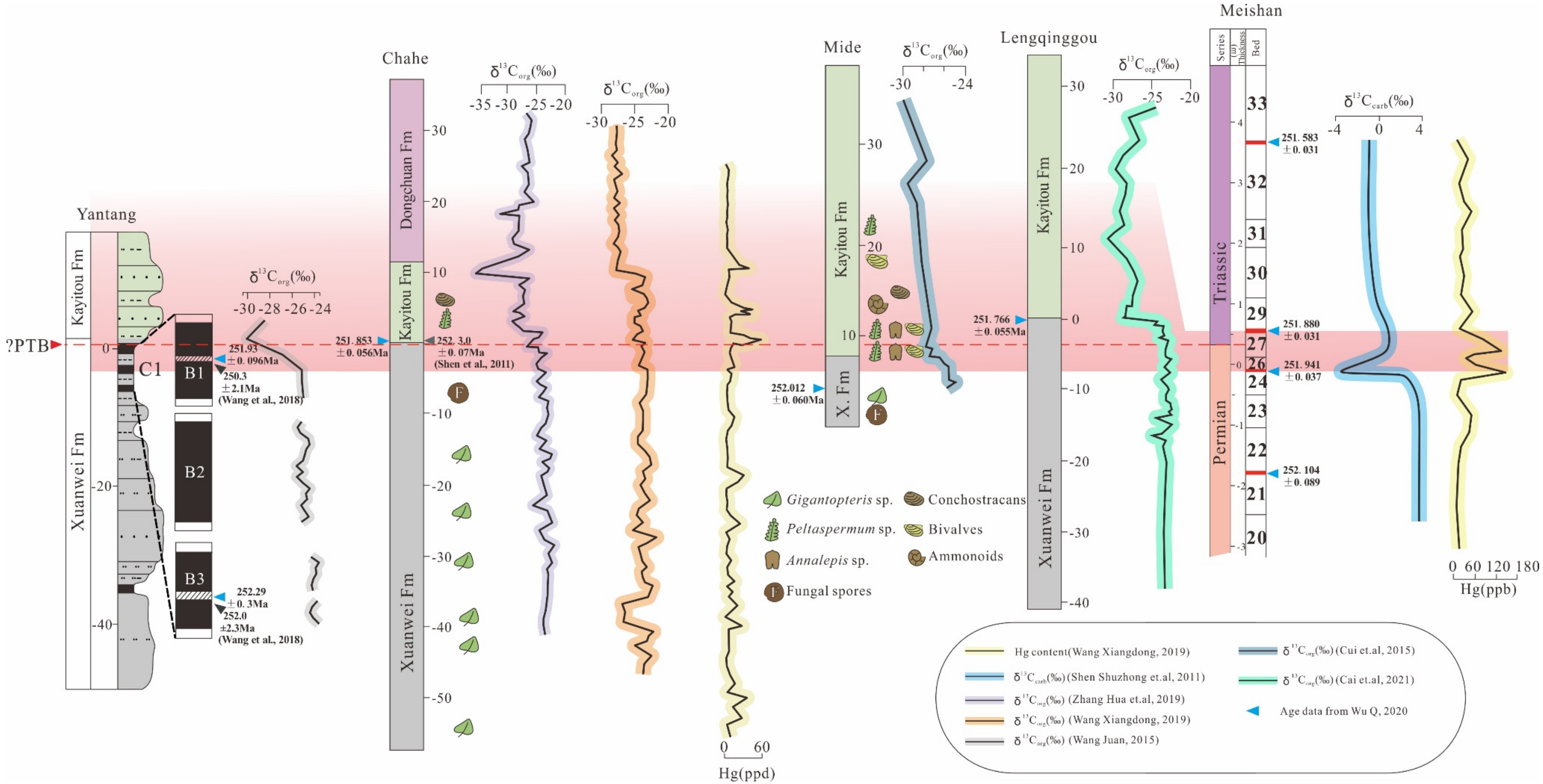

Fig. 1. Timing of the terrestrial end-Permian extinction event (occurrence of plant fossils after Bercovici et al., 2015)

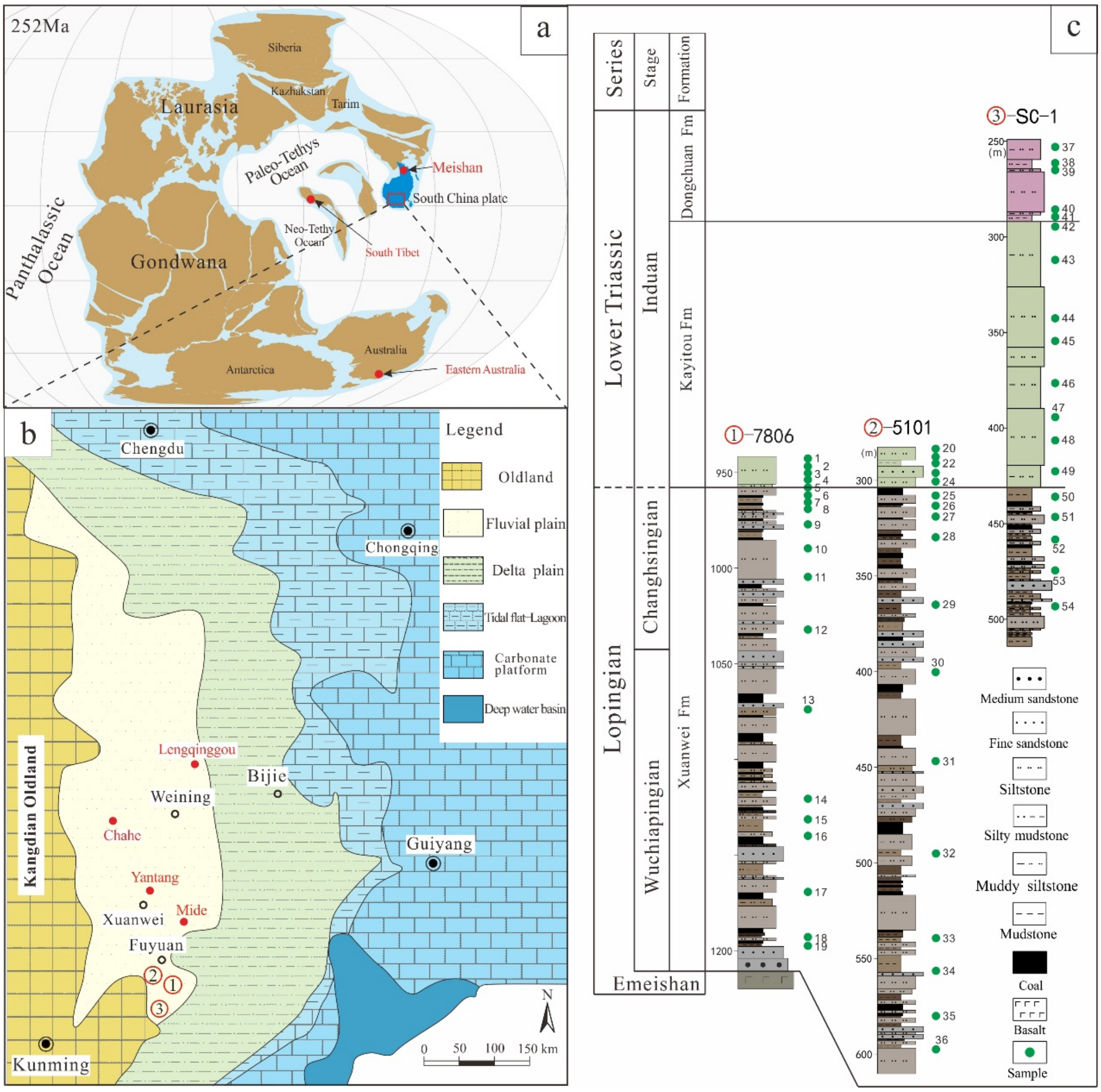

Fig. 2. Paleogeography of the Late Permian and stratigraphy of the Late Permian to the Early Triassic in southwestern China. a. Palaeogeographic configuration and the position of South China Plate (Huang et al., 2018), b. Paleogeography of southwestern China in the Changhsingian (Shao et al., 2013) and locations of the boreholes sampled; c. Lithology of the strata around the PTB and horizons of argillaceous rock samples in the boreholes.

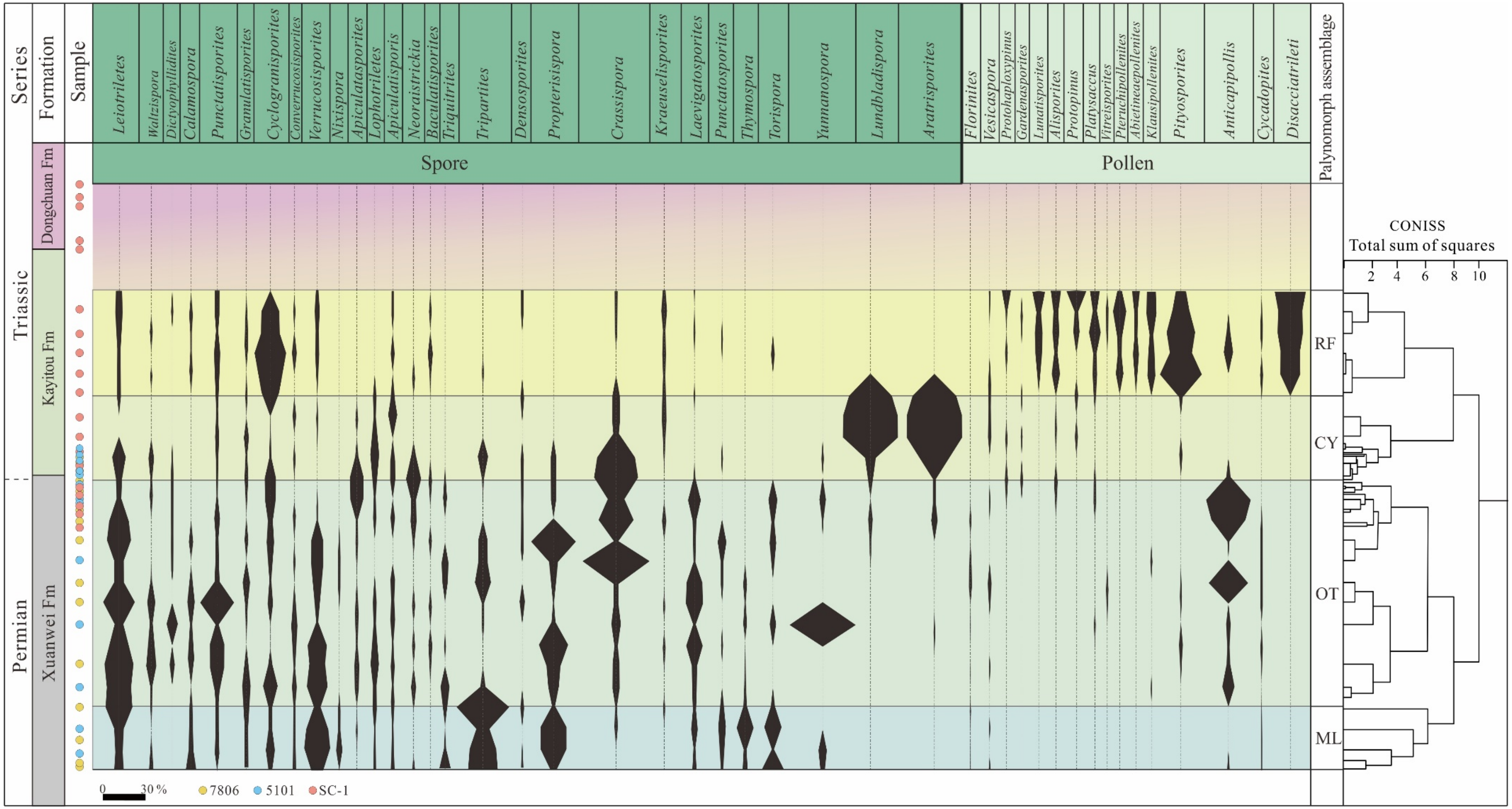

Fig. 3 Relative abundances of palynomorph taxa from the Late Permian to the Early Triassic in southwestern China.

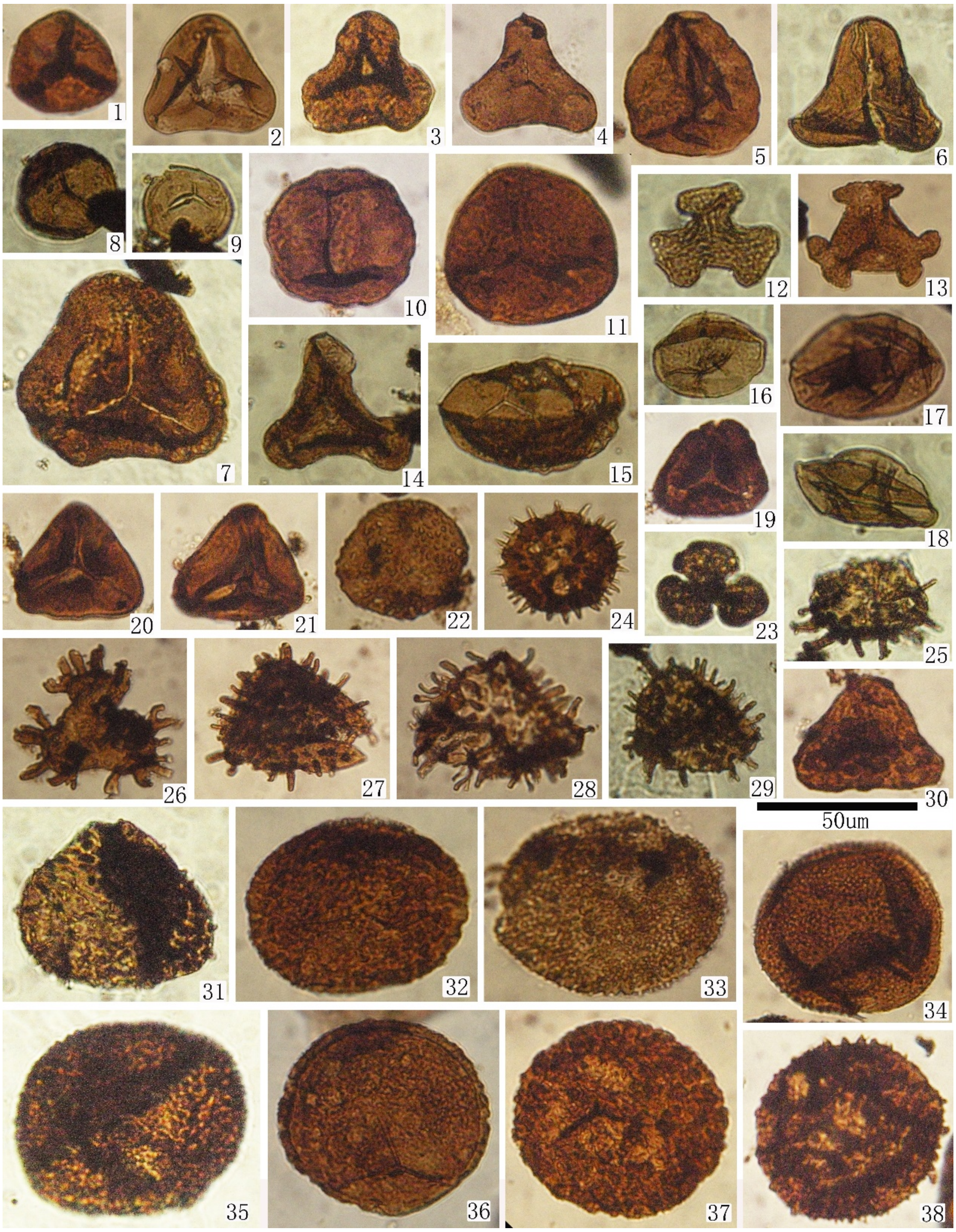

Fig. 4. Selected palynomorph taxa from ML assemblages. 1. *Leiotriletes ornatus* Ischenko, 1956；2. *Leiotriletes pulvinulus* Ouyang, 1986；3. *Leiotriletes adnatus* (Kosanke) Potonié and Kremp, 1955；4、6. *Leiotriletes concavus* (Kosanke) Potonié and Kremp, 1955；5. *Leiotriletes* sp.；7. *Leiotriletes cyathidites* Zhou, 1980；8、9. *Punctatisporites minutus* Kosanke, 1950；10. *Punctatisporites pistilus* Ouyang, 1986；11. *Punctatisporites* sp.；12、13. *Nixispora sinica* Ouyang, 1979；14. *Waltzispora strictura* Ouyang and Li, 1980；15. *Calamospora pallida* （Loose） Schopf, Wilson and Bentall, 1944；16、18. *Calamospora pusilla* Peppers, 1964；17. *Calamospora breviradiata* Kosanke, 1950；19、20. *Dictyophyllidites discretus* Ouyang, 1986；21. *Dictyophyllidites mortoni* (de Jersey) Playford and Dettmann, 1965；22. *Foveosporites*

foratus Ouyang, 1986；23. *Stellisporites inflatus* Alpern, 1958；24. *Baculatisporites* sp.；25. *Neoraistrickia* sp.；26. *Neoraistrickia spanis* Ouyang, 1986；27—29. *Raistrickia leptosiphonacula* Hou and Song, 1995；30. *Converrucosisporites confractus* Ouyang, 1986；31. *Lophotriletes* sp.；32、36. *Verrucosisporites ovimammus* Imgrund, 1952；33. *Verrucosisporites donarii* Potonié and Kremp, 1955；34. *Verrucosisporites microtuberosus* (Loose) Smith and Butterworth, 1967；35. *Verrucosisporites* sp.；37. *Schopfites phalacrosis* Ouyang, 1986；38. *Apiculatisporis variocorneus* Sullivan, 1964

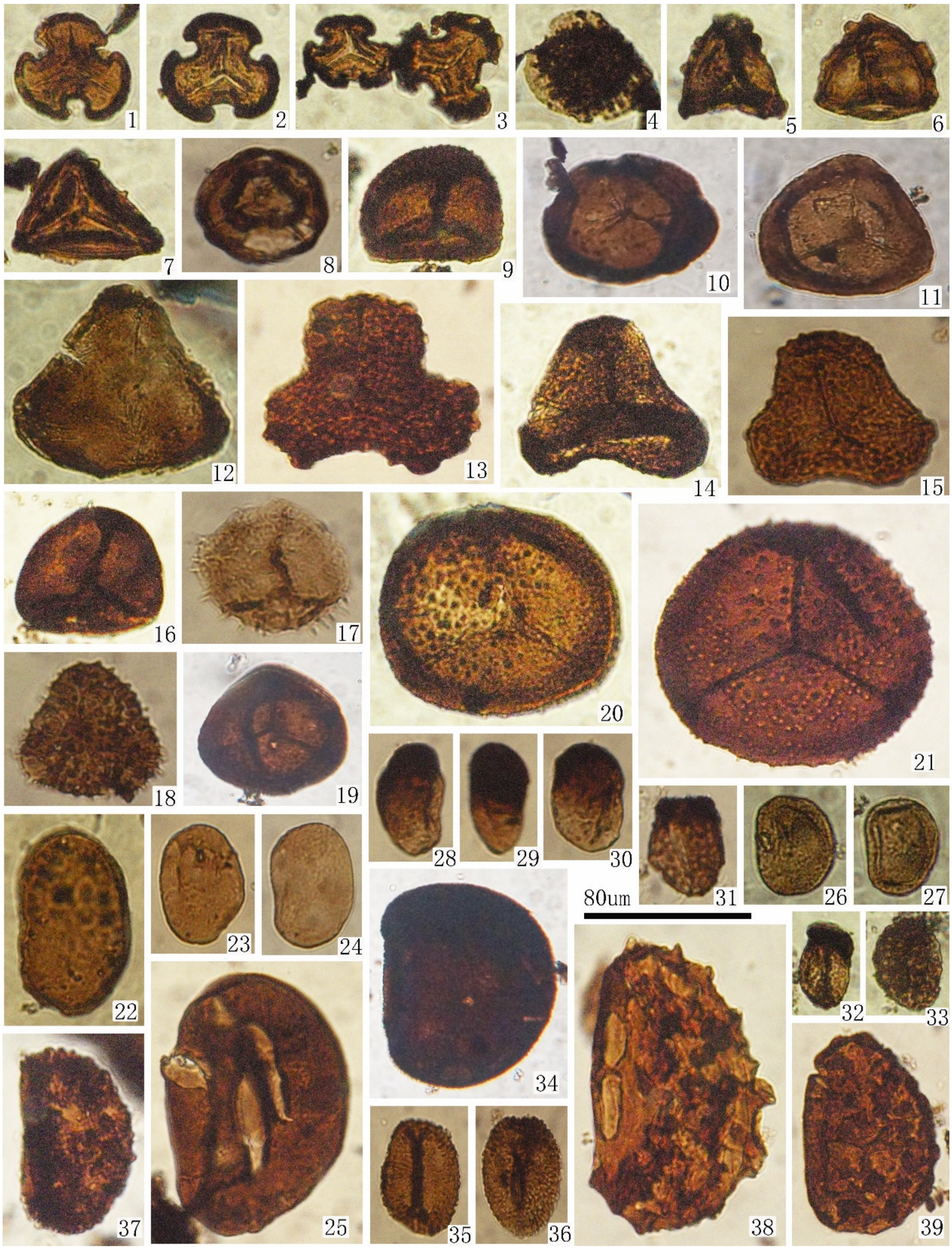

Fig. 5. Selected palynomorph taxa from OT assemblage. 1—3. *Tripartites cristatus* Dybova and Jachowicz var. *minor* Ouyang, 1986；4. *Rotaspora* sp.；5、6. *Propterisispora sparsa* Ouyang

and Li, 1980；7. *Propterisispora verruculifera* Ouyang, 1986；8. *Polycingulatisporites rhytismoides* Ouyang and Li, 1980；9. *Crassispora minuta* Gao, 1984；10. *Patellisporites meishanensis* Ouyang, 1962；11、19. *Densosporites paranulatus* Ouyang, 1986；12. *Triquitrites* sp.；13. *Triquitrites sinensis* Ouyang, 1962；14、15. *Triquitrites rugulatus* Ouyang, 1986；16. *Gulisporites cochlearius* (Imgrund) Imgrund, 1960；17. *Kraeuselisporites* sp.；18. *Acanthotriletes microspinosus* (Ibrahim) Potonié and Kremp, 1955；20、21. *Crassispora orientalis* Ouyang and Li, 1980；22. *Laevigatosporites vulgaris* Ibrahim, 1933；23、24. *Laevigatosporites minimus* (Wilson and Coe) Schopf, Wilson and Bentall, 1944；25. *Laevigatosporites maximus* (Loose) Potonié and Kremp, 1956；26、27. *Punctatosporites scabellus* （Imgrund） Potonié and Kremp, 1956；28－30. *Torispora laevigata* Bharadwaj, 1957；31. *Torispora verrucosa* Alpern, 1958；32. *Torispora securis* （Balme） Alpern, Doubinger and H。örst, 1965；33. *Thymospora mesozoica* Ouyang and Li, 1980；34. ？*Macrotoripora media* (Ouyang) Chen, 1978；35、36. *Yunnanspora radiata* Ouyang, 1979；37、39. *Polypodiidites fuyuanensis* Ouyang, 1986；38. *Polypodiidites reticuloides* Ouyang, 1986；

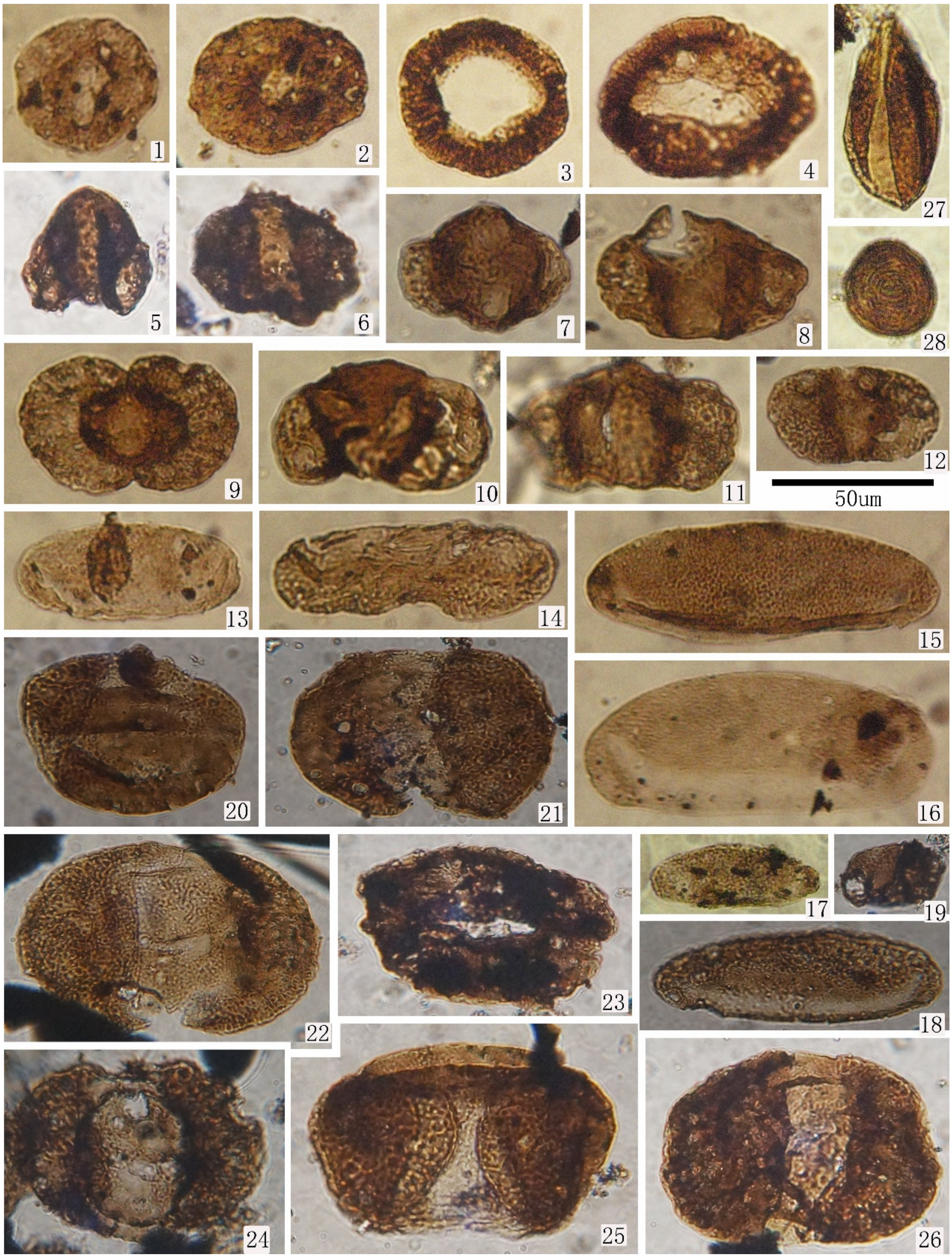

Fig. 6. Selected palynomorph taxa from CY assemblage. *Florinites relictus* Ouyang and Li, 1980；2. *Florinites mediapudens* (Loose) Potonié and Kremp, 1956；3. *Cordaitina rotata* (Luber) Samoilovich, 1953；4. *Cordaitina uralensis* (Luber) Samoilovich, 1953；5、7. *Alisporites auritus* Ouyang and Li, 1980；6. *Alisporites fusiformis* Ouyang and Li, 1980；8. *Klausipollenites* aff. *decipiens* Jansonius, 1962；9. *Platysaccus undulatus* Ouyang and Li, 1980；10、11. *Pteruchipollenites reticorpus* Ouyang and Li, 1980；12. *Pteruchipollenites caytoniformis* Zhou, 1980；13. *Anticapipollis rectangularis* Ouyang, 1986；14. *Cedripites lucidus* Ouyang, 1986；15、16. *Anticapipollis elongatus* Zhou, 1980；17、18. *Anticapipollis tornatilis* (Chen)

emend. Ouyang, 1979；19. *Vitreisporites pallidus* (Reissinger) Nilsson, 1958；20、22. *Lunatisporites* spp.；21、26. *Protohaploxypinus* sp.；23. *Gardenasporites meniscatus* Ouyang, 1986；24. *Protopinus fuyuanensis* Ouyang and Li, 1980；25. *Piceaepollenites* sp.；27. *Cycadopites* sp.

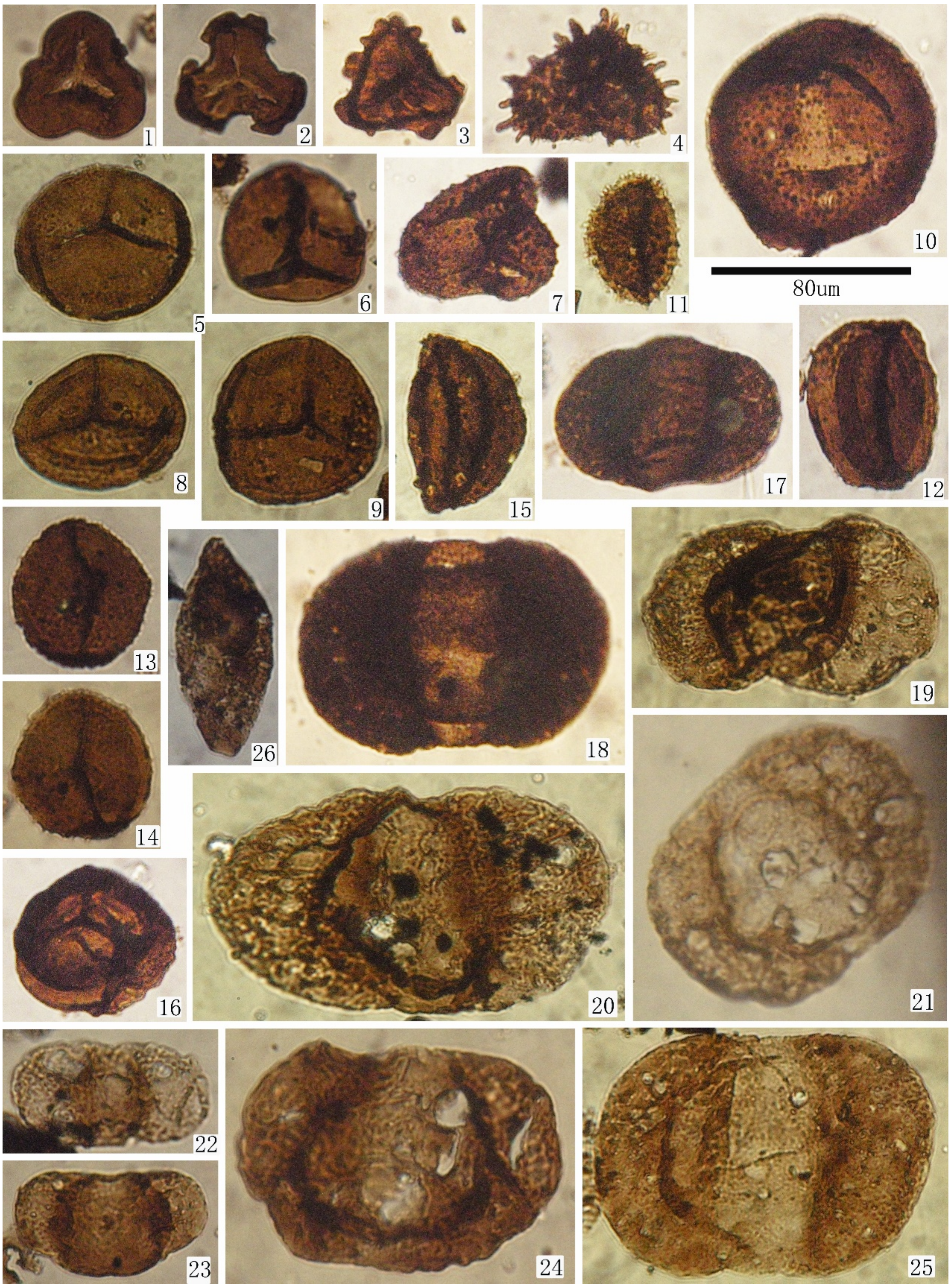

Fig.7. Selected palynomorph taxa from RF assemblage. *Leiotriletes adnatus* (Kosanke) Potonié and Kremp, 1955；2. *Tripartites cristatus* Dybova and Jachowicz var. *minor* Ouyang, 1986；3. *Propterisispora sparsa* Ouyang and Li, 1980；4. *Neoraistrickia irregularis* Ouyang and Li,

1980；5. *Punctatisporites* sp.；6. *Gulisporites cochlearius* (Imgrund) Imgrund, 1960；7. *Acanthotriletes microspinosus* (Ibrahim) Potonié and Kremp, 1955；8、9. *Lundbladispora subornata* Ouyang and Li, 1980；10. *Crassispora orientalis* Ouyang and Li, 1980；11、12、14. *Aratrisporites yunnanensis* Ouyang and Li, 1980；13. *Aratrisporites* sp.；15. *Striolatospora minor* Jiang, 1982；16. *Patellisporites meishanensis* Ouyang, 1962；17、18、24. *Lunatisporites* spp.；19. *Striatopodocarpites compressus* Ouyang and Li, 1980；20. *Vesicaspora* sp.；21. *Protopinus fuyuanensis* Ouyang and Li, 1980；22、23. *Pteruchipollenites reticorpus* Ouyang and Li, 1980；25. *Protohaploxypinus* sp.；26. *Cacadopites* sp.

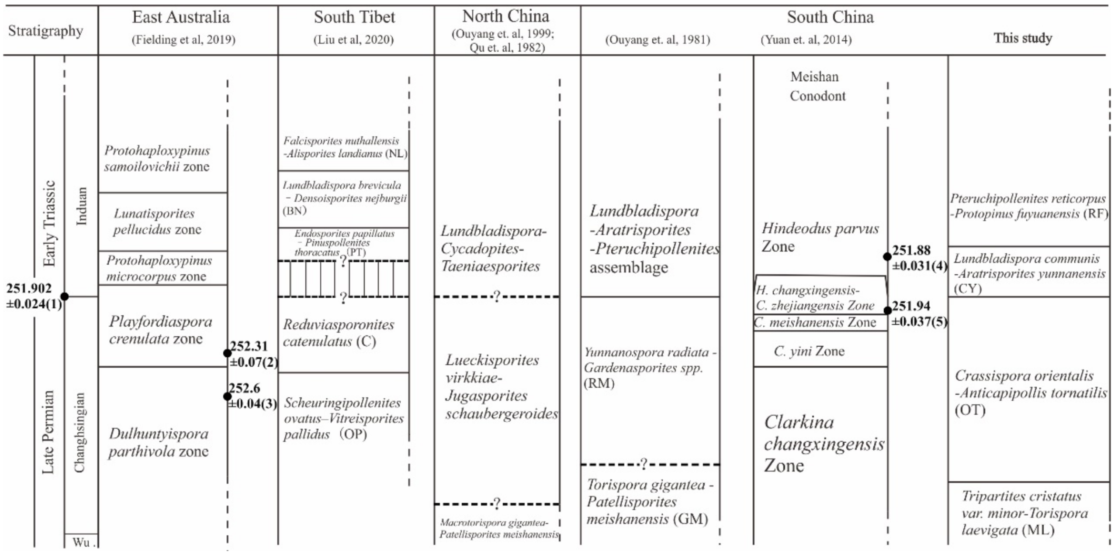

Fig. 8. Correlation of the Late Permian–Early Triassic palynostratigraphic scheme from southern Tibet with selected schemes. U/Pb ages (1), (4) and (5) from Burgess et al. (2014). U/Pb ages (2) and (3) from Fielding et al. (2019).

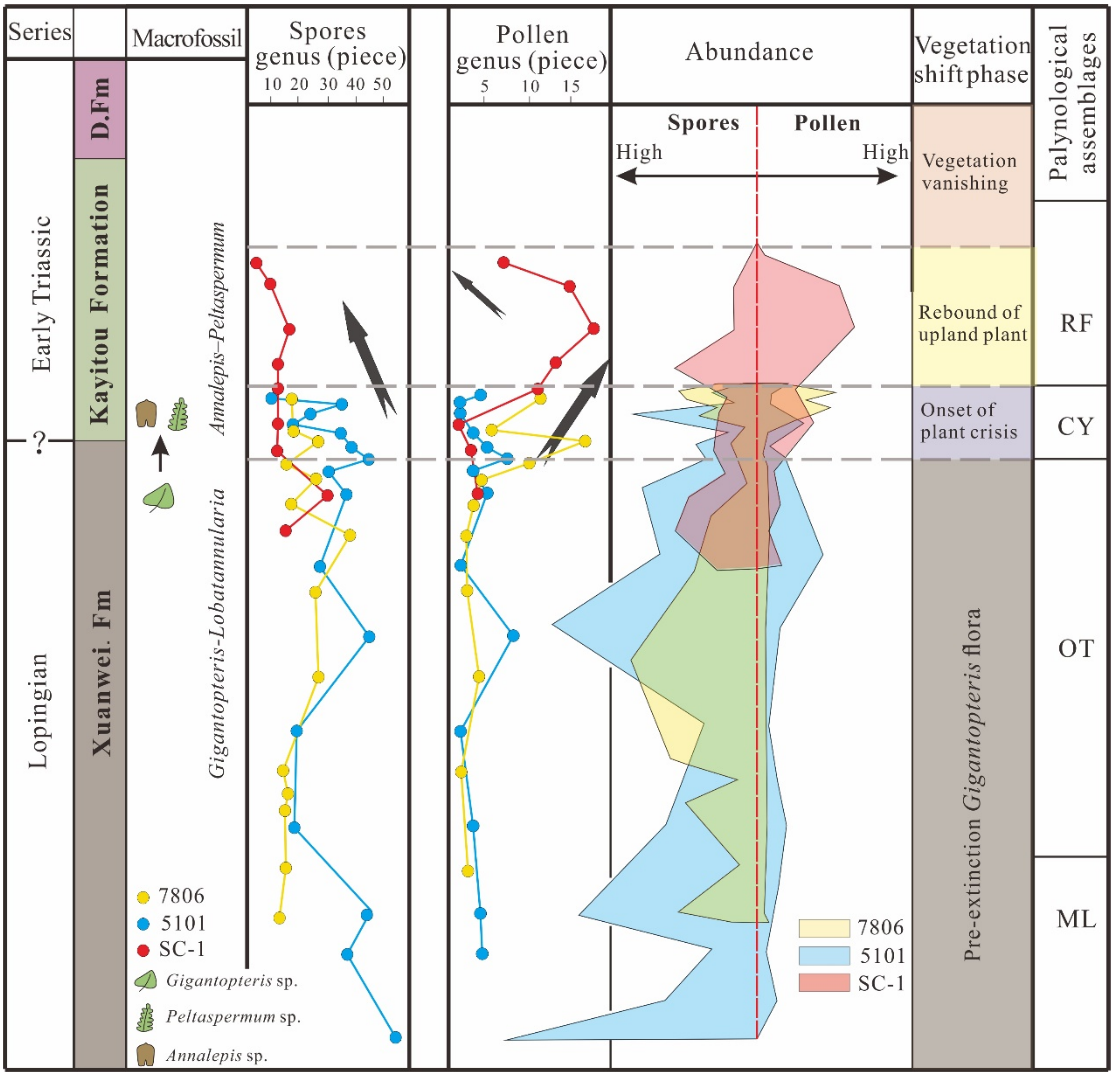

Fig. 9. Changes of palynology genus and abundance from the Late Permian to Early Triassic in southwestern China.

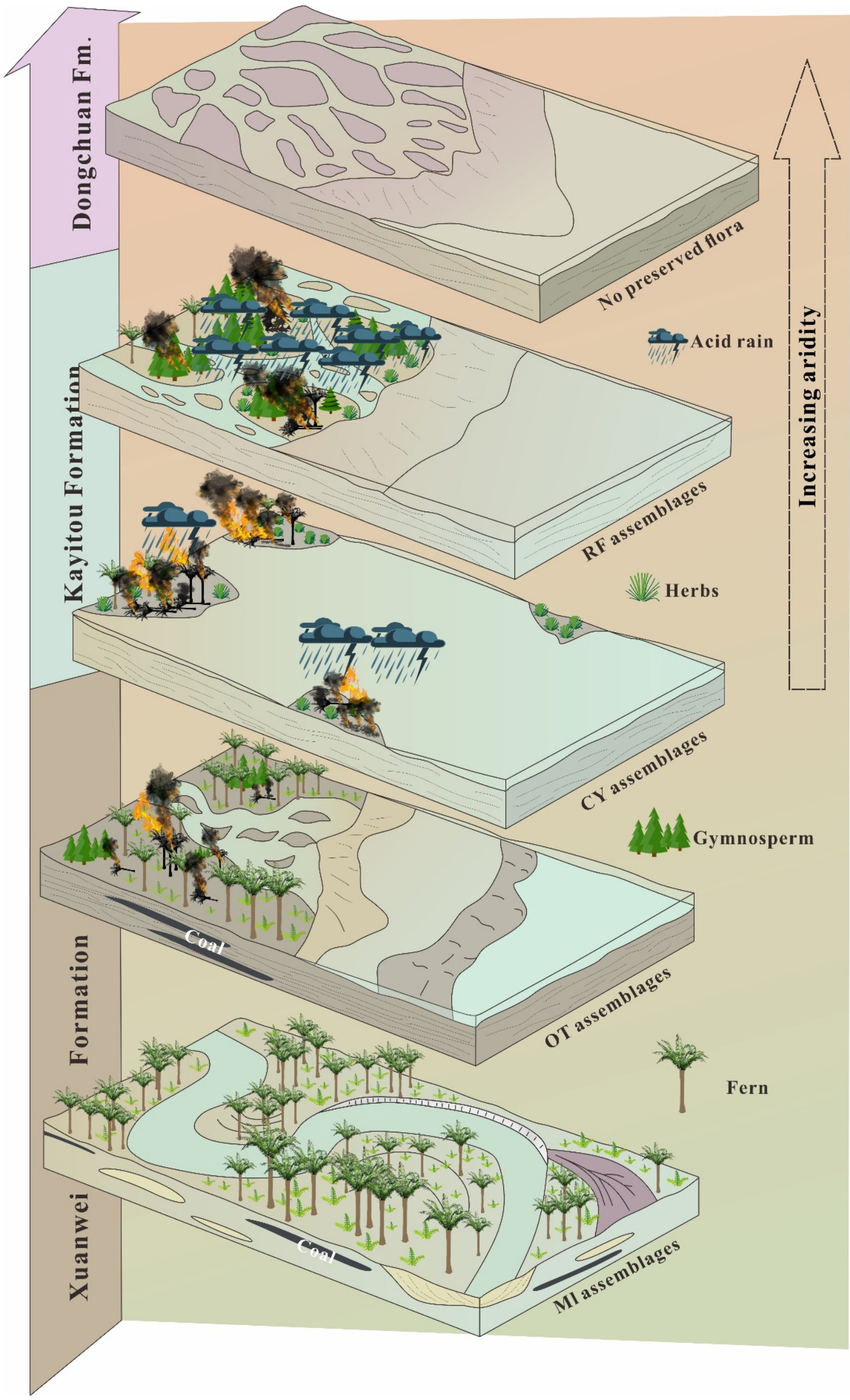

Fig. 10. Depositional models and paleobotanical evolution of southwestern China across the Permian–Triassic Boundary. Paleogeographic reconstructions for the Kayitou Formation and Dongchuan Formation were revised from Bercovici. et al. (2015)